Powder Metallurgy Progress, Vol.18 (2018), No.2, p.070-079
http://dx.doi.org/10.1515/pmp-2018-0008

WHAT WILL BE THE FUTURE OF POWDER METALLURGY?

Herbert Danninger

Abstract

Traditionally, powder metallurgy has been based on two major industrial sectors – ferrous precision parts and hardmetals. Both of them relied heavily on the automotive industry, with focus on internal combustion engines. Today, there is an increasing trend towards alternative drivetrain systems, and powder metallurgy faces the challenge to find new applications to replace those lost with the decrease of classical internal combustion drives. In this presentation it is shown that the main strength of powder metallurgy lies in its enormous flexibility regarding materials, geometries, processing and properties. This enables PM to adapt itself to changing requirements in a changing industrial environment. Examples given are PM parts in alternative drivetrain systems, new alloying concepts and processing routes offering distinct advantages. With hardmetals, innovative microstructures as well as sophisticated coatings offer increased lifetime, applications ranging from metalworking to rockdrilling and concrete cutting. A particularly wide area is found in functional materials which range from components for high power switches to such for fuel cells. Soft and hard magnets are accessible by PM with particularly good properties, PM having in part exclusivity in that respect, such as for NdFeB superhard magnets as well as soft magnetic composites (SMCs). Metal injection moulding (MIM) is gaining further ground, e.g. in the medical area which is a fast-growing field, due to demographic effects. Finally, most additive manufacturing techniques are powder based, and here, the knowledge in powder handling and processing available in the PM community is essential for obtaining stable processes and reliable products. Conclusively it can be stated that PM is on the way to fully exploit its potential far beyond its traditional areas of applications.

Keywords: Powder metallurgy, trends, precision parts, hardmetals, functional materials, additive manufacturing.

INTRODUCTION

Powder metallurgy is usually linked to two major product and application ranges – ferrous precision parts, mostly for automotive purposes [1-3], and hardmetals for tools [4, 5]. These product groups in fact make up for the major tonnage produced – PM parts – and the major turnover – hardmetals. Both product groups have started in the 1920s to 1930s and encountered tremendous growth after WW II, in particular with the expansion of automobile production, since the car industry is not only the major customer for precision parts, it also uses large quantities of hardmetal tools.

Herbert Danninger: Technische Universität Wien, Institut für Chemische Technologien und Analytik
A-1060 Vienna, Austria
Presented at "PM Auto 2018", April 16-18, 2018, Isfahan, Iran

With the increased skepticism towards the internal combustion engine – in part as a consequence of the "diesel crisis", resulting in diesel engines cars being banned from city centres - these traditional markets for PM parts are at least not as stable and predictable as they used to be. Electric or hybrid cars are subsidized by numerous governments and through they are still a small minority in the streets – except maybe from Norway - , it cannot be taken for granted that the internal combustion engine will be the main drivetrain at the end o the next decade. Therefore, the powder metallurgy industry has to be prepared for a fundamental change of its product range and its customer basis. The first to feel the change will be the ferrous parts manufacturers, but also other branches of PM will be affected by the change in car drivetrains.

On the other hand it must be remembered that one of the main features of powder metallurgy is its enormous flexibility regarding processes, materials, shapes and products [6]. In that respect, PM is like nature in which also many mutations occur, thus offering chances for survival also in a changing environment. Although the numbers for tonnages and turnover are dominated by the main product groups, there are numerous other PM products that are less spectacular quantitatively but are unbeatable qualitatively, PM being either the only or at least the most effective technique to manufacture them. In Fig.1 the variety of processes available in PM is graphically depicted.

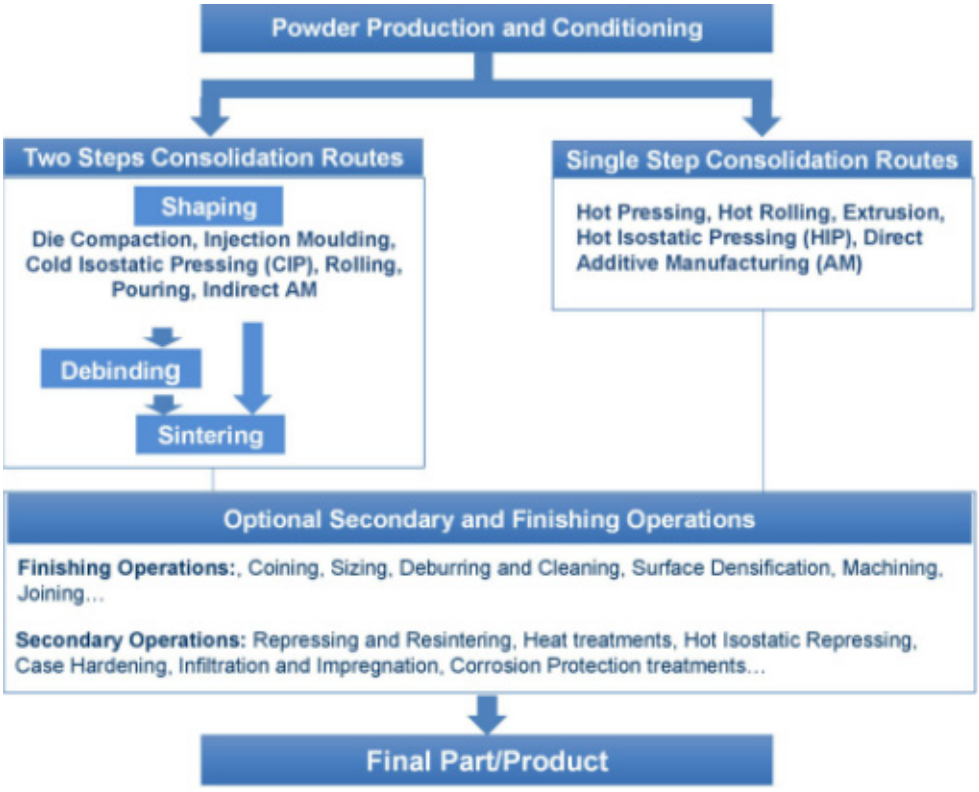

Fig.1. Powder metallurgy processing routes [6]

Furthermore, it must also be considered that many PM products offer high added value. This can already be seen when comparing ferrous parts with hardmetals; for the

former a price of 15.- EUR/kg can be estimated as an average while for the latter rather 200.- EUR/kg are calculated. Of course this includes the cost of the more expensive starting materials, but nevertheless.

When assessing PM products there are in principle 2 groups: those for which shape and precision are essential and those for which the material and its properties are the basis for existence. For the former, a camshaft belt pulley in an automotive engine is a good example, for the latter it is WC-Co hardmetal with its specific microstructure that is inaccessible e.g. by ingot metallurgy. Both examples are given in Fig.2.

a) Camshaft belt pulley (MIBA)

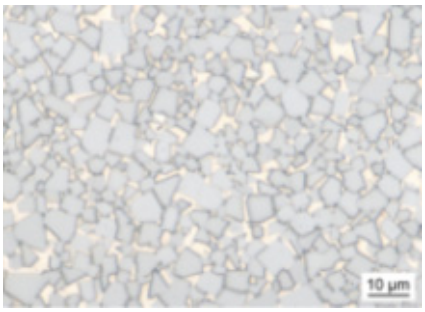

b) Microstructure of hardmetal

Fig.2. Examples of the major product groups of PM

In practice, both are frequently combined, as e.g. in hardmetal cutting inserts which exhibit not only the special microstructure of hardmetals but feature also intricate shapes and excellent geometrical precision. Other examples are self-lubricating bearings and filters.

In the present article, several product groups of PM – by far not all of them - are discussed, from traditional parts to additive manufactured components, and their perspectives are estimated as far as this is possible today.

FERROUS PRECISION PARTS

Today, sintered precision parts are used to a large extent in classical internal combustion engines and transmissions. However, also alternative drivetrain systems such as add-on hybrids need a sort of transmissions, components for which are accessible through powder metallurgy [7, 8]. In particular for electrically driven vehicles, the noise-damping capacity of PM gears might be a definite asset since without the noise caused by the internal combustion engine, other sources of unwelcome noise become prominent [9]. Also the trend to downsizing of combustion engines is favourable for PM, applications such as clearance-free gears and camphasers for the camshaft drive being already in service here (Fig.3).

A very important feature is the increasing load-bearing capacity of ferrous PM parts. This is in part due to material development, new alloying systems being used [10]. Here, in particular cost-effective and non-toxic alloy element, such as Cr, Mn and Si are attractive. PM steels such alloyed are more difficult to sinter, as a consequence of the high oxygen affinity of the alloy elements [11, 12], but today the sintering furnace as well as the atmospheres can afford the required cleanliness of the sintering environment regarding oxidizing compounds, and at sufficiently high sintering temperatures which are desirable anyhow regarding the mechanical properties – also fairly stable oxides are reduced.

a) Clearance-free PM gear b) Camphaser stator c) Camphaser rotor

Fig.3 PM components for modern internal combustion engines (MIBA Sinter Austria)

In particular Cr is introduced mainly through the prealloying route since this element does not too much affect the compressibility of the powder. With Mn and Si this is more of a problem. An elegant method to introduce these elements is the masteralloy route, i.e. using a base iron powder – with excellent compressibility – and adding the alloy elements though a fine high-alloy powder that contains the desired elements in combination with Fe. By this way the compositional flexibility is superior to the prealloyed grades while the oxygen affinity is lowered by the lower chemical activity of the alloy elements. Using e.g. Fe-Mn-Si masteralloys, sintered steels with excellent properties can be attained [13].

A further, already established, way to improve the load bearing capacity in particular of PM gears is surface densification by rolling, e.g. [14]. By this method, the mechanically loaded tooth flanks and roots obtain the load-bearing capacity of a fully dense steel while the remaining part is porous, thus being 10-15% lighter than a fully dense steel part and also offering better NVH (noise-vibration-harshness) behaviour. Surface rolling is usually combined with thermochemical treatment, low pressure carburizing being particularly suitable here since the carburizing depth is hardly affected by porosity, and thus the fully dense functional surfaces can be properly carburized without overcarburizing the porous faces, which would hardly be possible by standard gas carburizing [15,16].

HARDMETALS

With hardmetals, the classical WC-Co type is still absolutely dominating, despite objections about the availability of W and the frequently temperamental behaviour of the Co price. However, since Co has been classified cancerogenic by the EU, at least increased cost must be expected by the hardmetal industry. Alternative binders have been studied for a long time, but replacing Co by the equally critical Ni is not the optimal solution, and Fe based binders suffer from a very narrow two-phase region, which makes proper carbon control extremely tricky [17]. Furthermore, also the phase stability of the Fe-based binder is an aspect to be considered, phase transformations during service being usually undesirable. Therefore, WC-Co will remain the standard hardmetal base at least for the next years to come.

Hardmetals based on other hard phases than WC, usually TiCN, the so-called cermets, have been used for decades, but have found widespread application only in Japan, in Europe and North America the market share is below 20%. The main incentive, a possible scarcity of W, is not a problem today, also as a consequence of systematic recycling of spent cutting tools and of the more focused use of hardmetals, this expensive material being used only where it is really needed, e.g. just on the tips of rock drills (Fig.4).

Hardmetals are less dependent on the automotive industry, esp the internal combustion engine, than are ferrous PM parts. Although the carmakers are important customers, e.g. machining of jet engines consumes a lot of HM inserts, as do rock drilling and concrete cutting (Fig.4).

Fig.4 Hardmetal-tipped rock drill (HILTI AG)

From the material viewpoint, ultrafine hardmetal grades tend to further grow in market share [18]. In particular for metal cutting, coatings applied by PVD or CVD consistently increase cutting performance and lifetime [19], thus enabling economical machining of tricky materials such as heat treated steels, Ti base materials or Ni base superalloys.

REFRACTORY METALS

This group of metals has been at the beginning of modern PM, the main product at that time being W lamp filaments [20]. In these early days, attaining the melting temperature of these metals was not possible technically, PM being the only feasible route. Currently, melting also of W is possible, However, also today, PM is the main production route for W, Mo and Ta [21], the microstructures obtained by PM being more favourable than those of ingot metallurgy specimens. This holds still more for refractory-based pseudoalloys, i.e. two-phase materials such as W heavy alloys or W-Cu contact materials, and these very special but essential groups of materials will be used also in the future. Fig.5a shows a heavy alloy collimator for radiotherapy, while Fig.5b depicts contacts for high voltage/high current switched tipped with W-Cu pseudoalloys which are inaccessible by other means than PM. For medium voltage vacuum switches, Cu-Cr contacts are used which can also be produced by ingot metallurgy routes; here, however, the shaping capability of PM is a distinct advantage for manufacturing the very complex contact ends of these switches.

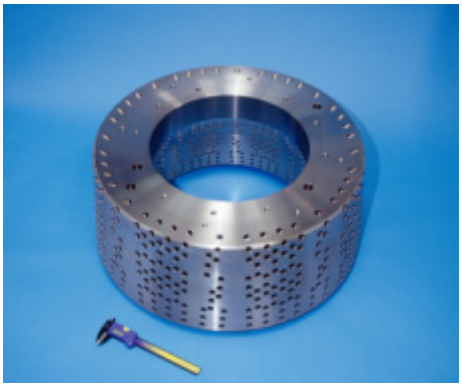

Fig.5a Heavy alloy collimator for radiotherapy (mass approx. 2 tons)(Plansee SE).

Fig.5b W-Cu-tipped contacts for high voltage/high current switches (Plansee SE).

Another application for PM refractory metals and superalloys are components for solid oxide fuel cells [22], the metal-based SOFCs being more robust mechanically than e.g. anode or electrolyte-supported variants. Here, Cr interconnects have been manufactured by the press-and-sinter route, as have been supports with defined, open and

interconnected porosity for introducing fuel and oxygen as well as removing the reaction products. In this case, the capability of PM to manufacture metallic bodies with well defined and regular porosity is a distinct advantage.

METAL INJECTION MOULDING, MIM

The MIM is a success story of powder metallurgy, exhibiting sales growth rates of about 10% annually in the last decades; not even the crisis of 2008 had much impact here. The combination of the geometrical flexibility of polymer injection moulding with the material flexibility offered by PM has shown to be highly attractive for numerous applications, such as machinery, medical, automotive, [23, 24]. In Figure 6 some examples are given.

In the MIM, the major fraction of the products still consist of stainless steel, but also low alloy steels, hardmetals and Ti base materials are used, the difficulties associated with the tendency of Ti to absorb O, N, C and H into the lattice, with resulting embrittlement, having been overcome. Also MIM of Mg is being studied, as a consequence of the difficulties to obtain intricate-shaped Mg parts by machining. MIM of Al is still in the experimental state, but encouraging results have been reported, the main problem being complete removal of carbon rather than the oxide layers on the Al powder particles [25].

Fig.6a MIM parts for machinery (itb)

Fig.6b MIM parts for automotive (GKN)

Fig.6c MIM parts for bicycles (OBE)

Fig.6 Examples of MIM Parts (Courtesy Fraunhofer IFAM).

PM MAGNETIC MATERIALS

Today, by far the major proportion of the total tonnage of soft magnetic materials (18.5 Mto) consists of electrical steel sheet, either isotropic (81%) or oriented (14.5%)[26]. Only 4.5% make up for the rest, such as FeNi, FeCo, ferrites, ... Once more, however, PM is an attractive route for special products. This may include shaped soft magnetic parts obtained by the press-and-sinter route [27]; here, Fe, Fe-P, Fe-Si and Fe-Si-P are common materials. The role of porosity on the magnetic properties is fairly well known today, for soft magnetic parts the coercive force being particularly critical.

One advantage of PM is that the poor deformability of Fe-Si with >4%Si does not play a role with sintered materials if starting from powder mixes. The homogenization of Si in the matrix during sintering is strongly enhanced by the ferrite-stabilizing effect of Si, i.e. the homogenization is a self-accelerating process. Another material for which the shaping capability of PM is a definite asset is Fe-Co, the magnetic material with the highest saturation magnetisation but with very poor mechanical properties and machinability (“Crackalloy”). Using the net shape production by PM is a clear benefit here.

A clearly unique group of materials are the so-called soft magnetic composites (SMCs), which are attractive for AC applications at high frequencies. Alternating magnetic

fields, as induced by AC, cause eddy currents in electrically conductive materials that result in energy losses by heating. Traditionally this is remedied by using laminated steel sheets – each sheet being electrically insulated from its neighbours - , as common e.g. in transformer cores, but their efficiency markedly decreases at higher frequencies. SMCs, in contrast, consist of powder particles which are electrically insulated by a surface layer. The powders are coated by organic or inorganic layers, then pressed and cured or annealed, but not sintered. In order to keep the resistivity as high as possible – to keep eddy current losses low - ´damage to the insulating layers during pressing or curing/annealing has to be minimum, and for low coercive force, annealing has to be done to eliminate work hardening due to pressing but without damage to the insulating layers, which compromise is not easy to be found.

The SMCs compete with laminated steel sheet [26, 28]: at lower frequencies the laminates are superior with regard to magnetic properties, mainly because of the better saturation as a consequence of being fully dense; at higher frequencies, in contrast, SMCs offer benefits because of their higher resistivity. However, also the shaping capability of the PM route has to be considered; complex-shaped parts are more easily produced as SMC. Also 3-dimensional magnetic flux can be easily realized using SMCs. Although SMCs have been known and investigated for about 20 years, today, with the increasing trend to electrical drives, it has become also industrially attractive, and all major PM manufacturers are working on this topic.

On the other end of the ferromagnetic product range are the superhard (rare earth) magnets, based mainly on NdFeB. Here, PM is the exclusive production method [29], although the very high oxygen affinity of Nd makes the handling of powder tricky to avoid undesirable oxygen pickup. Both monolithic (= sintered) and polymer-bonded NdFeB magnets have been on the markets for a number of years, consolidation in the magnetic field being standard; recently, also production e.g. by MIM has been done, and additive manufacturing has been tried [30]. The problem of raw materials supply, exaggerated by the fact that China is the principal – and almost exclusive – supplier of RE elements such as Nd and Dy, is being tackled by developing recycling techniques that enable reclaiming at least a significant fraction of the RE magnets used in Europe and America. Also for new, RE-free hard magnetic materials such as FePt, CoPt and MnAl, PM manufacturing offers interesting perspectives.

ADDITIVE MANUFACTURING

Today, AM, also known as 3-D-printing, is the most rapidly expanding manufacturing technology, and a very large proportion of it is powder based. The Figure 7 shows the different variants of AM; and it is evident how many routes are available there. For many of them, metal powders are the starting materials, and powder knowhow is therefore essential for successful production. AM enables manufacturing of structures that are inaccessible by other techniques, at least without complicated joining processes [31].

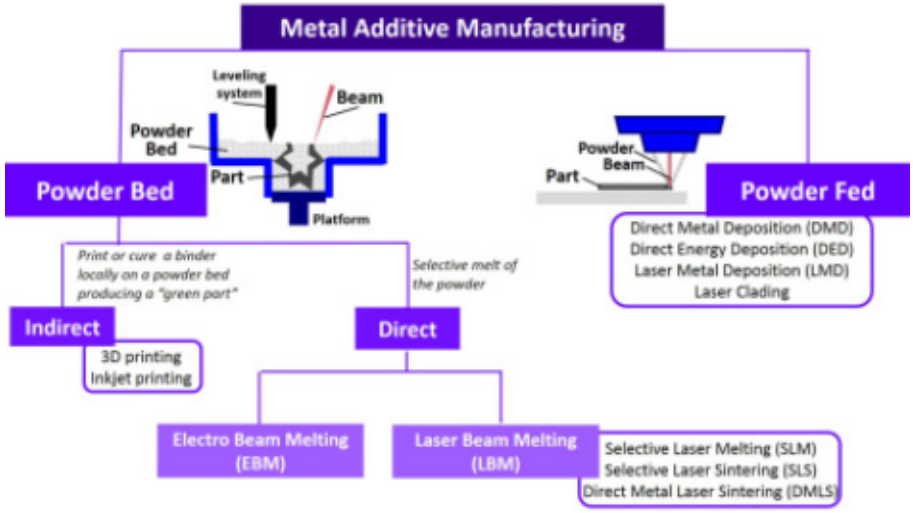

Fig.7. Variants of Additive Manufacturing routes for metallic products [6].

Today it is mostly the direct processes that are in the focus of public attention, in particular Direct Laser Melting (DLM) and Electron Beam Melting (EBM), since the aerospace components thus produced are in part already in service which is widely publicized. In Fig. 8 some components manufactured by DLM are shown.

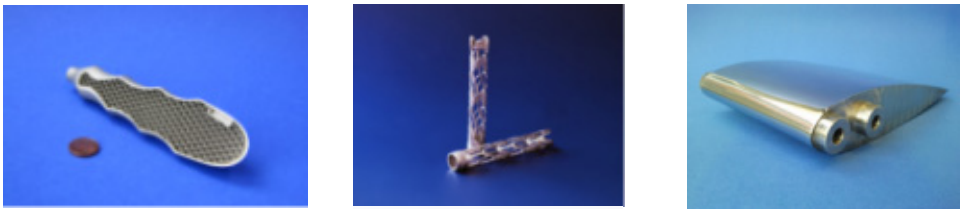

a) Handle for medical tool b) Stent c) Hollow airfoil

Fig.8. Components manufactured by Direct Laser Melting (Fraunhofer IFAM Bremen).

However, also the indirect techniques which use organic binders to consolidate the powder assembly, such as inkjet printing, photolithography or screen printing, offer benefits. Although they need further steps such as debinding and sintering, the isothermal processing lowers the risk of distortion – which is very critical with the direct processes - , and much experience gained from MIM can be used. Also the option of implementing a desired surface finish before sintering should be acknowledged. Finally, the AM equipment for the indirect processes is in part significantly cheaper than DLM or EBM machines.

In any case it can be predicted that the Additive Manufacturing techniques will gain further ground in the future, and PM knowhow will be essential here. Applications will be widespread, from automotive [32] to aerospace [33] and many others There are several open questions, e.g. the effect of recycling powders or feedstock [34], the fatigue properties and how the required surface quality can be attained in an economical way. However, regarding the huge number of research groups and the money invested it can be expected that these problems will be solved in the near future, e.g. by combining AM with other techniques such as HIP [35].

CONCLUSIONS

In general the following predictions can be made:

- Combining special material and net shape technologies will become still more important, to ensure production with minimum material and energy consumption
- In the years to come, classical PM precision parts will be further used in automotive drivetrains, new opportunities being found both in downsized combustion engines and in alternative drive systems such as hybrids.
- PM functional materials will gain more and more importance, esp. for electrical and magnetic applications
- This holds in particular for Soft Magnetic Composites; in this field the primary mover for further development originates from the sector electromobility.
- Powder based additive manufacturing processes will make further progress and will find increasingly use in practice; this holds for both the direct and the indirect manufacturing routes.
- In addition to the classical direct processes such as Direct Laser Melting and Electron Beam Melting, also indirect, i.e. metal powder + binder-based routes will find increasing use, in part because of the more cost efficient equipment.
- As with other manufacturing techniques, also for PM tools for simulation and modelling will find increasing use, also because of more reliable and comprehensive input data being available.

Acknowledgement

The author wishes to thank the following persons for supplying information and images: Magdalena Dlapka, MIBA Sinter Austria; Gerd Kotthoff, GKN Sinter Metals; Frank Petzoldt and Claus Aumund-Kopp, Fraunhofer-IFAM Bremen; Bernd Kieback, Fraunhofer-IFAM Dresden; Andreas Schoppa, PMG; Lorenz Sigl, Plansee SE; Steven Moseley, HILTI AG; Raquel de Oro Calderon, TU Wien.

REFERENCES

[1] Williams, B.: Powder Metall. Review, vol. 5, 2016, no. 4, p. 47
[2] Silbereisen, H.: Powder Metall. Int., vol. 16, 1984, no. 2, p. 65
[3] Whittaker, D.: Powder Metall. Review, vol. 4, 2015, no. 2, p. 35
[4] Brookes, KJA.: Hardmetals and other Hard Materials. 2nd ed. East Barnet UK : Int. Carbide Data, 1992
[5] Schubert, WD., Lassner, E., Boehlke, W.: Cemented carbides – a success story. London : International Tungsten Industries Association, 2010
[6] Danninger, H., De Oro Calderon, R., Gierl-Mayer, C. In: Ullmann's Encyclopedia of Industrial Chemistry. Wiley-VCH, Online 2017, p. 1
[7] Kotthoff, G., Leupold, B., Janzen, V. In: Pulvermetallurgie in Wissenschaft und Praxis. Vol. 33. Eds. H. Kolaska, H. Danninger, B. Kieback. Hagen : Fachverband Pulvermetallurgie, 2017, p. 185
[8] Flodin, A.: Powder Metall. Review, vol. 6, 2017, no. 2, p. 41
[9] Dlapka, M., Müller, A. In: Pulvermetallurgie in Wissenschaft und Praxis. Vol. 33. Eds. H. Kolaska, H. Danninger, B. Kieback. Hagen : Fachverband Pulvermetallurgie, 2017, p. 207
[10] Danninger, H., Gierl, C.: Sci. Sintering, vol. 40, 2008, no. 1, p. 33
[11] De Oro Calderon, R., Gierl-Mayer, C., Danninger, H.: Journal of Thermal Analysis and Calorimetry, vol. 127, 2017, no. 1, p. 91
[12] Gierl-Mayer, C., De Oro Calderon, R., Danninger, H.: JOM, vol. 68, 2016, no. 3, p.

920
[13] De Oro Calderon, R., Gierl-Mayer, C., Danninger, H.: Powder Metallurgy, vol. 59, 2016, no. 1, p. 31
[14] Jones, PK., Buckley-Golder, K., Sarafinchan, D.: Int. J. Powder Metallurgy, vol. 34, 1998, no. 1, p. 26
[15] Dlapka, M., Gierl, C., Danninger, H., Altena, H., Stetina, G., Orth, P. In: Proceedings PM2010 Powder Metallurgy World Congress & Exhibition, Florence. Vol. 2. Shrewsbury : European Powder Metallurgy Association, 2010, p. 459
[16] Mulin, H., Giraud, Y., Since, JJ.: Powder Metall. Review, vol. 3, 2014, no. 2, p. 61
[17] Schubert, WD., Fugger, M., Wittmann, B., Useldinger, R.: Int. J. Refr. Metals & Hard Mater., vol. 49, 2015, p. 110
[18] Schubert, WD.: Keramische Zeitschrift, 2015, no. 7, p. 365
[19] Garcia, J. et al.: Adv. Eng. Mater., vol. 12, 2010, p. 929
[20] Johnson, PK.: Int. J. Powder Metall., vol. 44, 2008, no. 4, p. 43
[21] Leichtfried, G. In: Landolt-Börnstein New Series VIII/2A2 “Refractory, Hard and Intermetallic Materials”. Chapter 12. Berlin-Heidelberg : Springer, 2002, p. 1
[22] Haydn, M., Ortner, K., Franco, T., Menzler, NH., Venskutonis, A., Sigl, LS.: Powder Metall., vol. 56, 2013, no. 5, p. 382
[23] German, RM.: Adv. Powder Metall. & Partic. Mater. Part 4. Princeton NJ : MPIF, 2011
[24] Johnson, PK.: Int. J. Powder Metall., vol. 52, 2016, no. 1, p. 5
[25] Gierl, C. et al.: Powder Injection Moulding International, vol. 6, 2012, no. 4, p. 65
[26] Schoppa, A., Delarbre, P. In: Pulvermetallurgie in Wissenschaft und Praxis. Vol. 29. Ed. H. Kolaska. Hagen : Fachverband Pulvermetallurgie, 2013, p. 231
[27] Dougan, M.: Powder Metall. Review, vol. 4, 2015, no. 3, p. 41
[28] Schoppa, A., Delabre, P., Holzmann, E., Silg, M. In: Proc. IEEE EDPC Conf. Nuremberg, 2013
[29] Narasimhan, KS.: Powder Metall. Review, vol. 6, 2017, no. 4, p. 47
[30] Burkhardt, C. In: Proc. EuroPM2017 Milan. Shrewsbury : EPMA, 2017
[31] Isaza, JF., Aumund-Kopp, C.: Powder Metall. Review, vol. 3, 2014, no. 2, p. 41
[32] Anonymous: Metal Additive Manuf., vol. 2, 2016, no. 2, p. 32
[33] Bhate, D.: Metal Additive Manuf., vol. 3, 2017, no. 3, p. 81
[34] Hryha, E., Shvab, R., Gruber, H., Leicht, A., Nyborg, L. In: Proc. EuroPM2017 Milano. Shrewsbury : EPMA, 2017, paper no. 3687558
[35] Whittaker, D.: Metal Additive Manuf., vol. 3, 2017, no. 4, p. 83

Powder Metallurgy Progress, Vol.18 (2018), No.2, p.080-095
http://dx.doi.org/10.1515/pmp-2018-0009

STUDYING THE PROGRESS OF SINTERING IN FERROUS POWDER COMPACTS BY IN-SITU MEASURING THE THERMAL CONDUCTIVITY

H. Danninger, G. Leitner, Ch. Gierl-Mayer

Abstract

In situ characterization of the sintering process is a difficult task, in particular for systems without pronounced dimensional changes. Dilatometry is not too helpful in those cases, and therefore other properties have to be recorded. In the present study, sintering of ferrous powder compacts was studied in situ by measuring the thermal diffusivity ***a*** *using a laser flash apparatus. This property is a measure to characterise the heat flow through a material; it depends on the contact area between the particles and thus reveals their change during sintering. It is shown that the change of* ***a*** *during sintering of ferrous compacts is much less pronounced than in the case of cemented carbides which is not surprising when regarding the widely differing porosity changes. The results are however in good agreement with expectations when considering some experimental limitations. The trend for the thermal conductivity λ. which can be calculated from* ***a****, the specific heat and the density, is in good agreement with that found for the electrical conductivity, both properties being linked through Wiedemann-Franz' law.*

Keywords: Sintered steels; sintering; in-situ characterization; laser flash; thermal diffusivity

INTRODUCTION

Both for scientific research and for stable and reliable industrial production, the basic processes occurring during the sintering cycle have to be known. The traditional route to study sintering is to perform runs under varying parameters such as temperature, time and atmosphere and then cooling or quenching the specimens with subsequent investigation such as mechanical testing, metallography etc. This can be done as stepwise sintering or through interrupted runs. These indirect methods however give only indirect information about the progress of sintering; a result is obtained but is cannot immediately be stated during which step of sintering this result has been obtained. Furthermore, e.g. for simulating the sintering process the properties at a given temperature are of relevance and have to be known [1].

Herbert Danninger, Christian Gierl-Mayer: Technische Universität Wien, A-1060 Wien/Vienna, Austria
Gert Leitner: retired; formerly Fraunhofer-Institut für Keramische Technologien und Systeme (IKTS), D-01277 Dresden, Germany

Direct characterization of sintering is decidedly more informative. So far, mainly the various methods of thermal analysis such as dilatometry [2], thermogravimetry, differential thermal analysis/scanning calorimetry, in part combined [3] and also linked to chemical analysis such as mass spectrometry [4], have been used. These methods give valuable insight into dimensional changes, enthalpy changes, and chemical reactions occurring during sintering. However they do not yield information about microstructural changes such as formation and growth of sintering contacts. An interesting approach has been made by Shoales [5] who measured the strength of specimens in various stages of the sintering process and could find relationships to distortion. However, each measurement consumes one specimen. For studying the distortion, also optical methods have been applied [6], but these just give the macroscopic results but not so much the microstructural background.

For studying the formation and growth of sintering contacts e.g. in PM steels, measuring the electrical conductivity $\boldsymbol{\kappa}$ has been proposed quite early, both from the as sintered samples [7] and also in-situ (e.g. Ritzau, in [8]). Conductivity is quite directly linked to the effective load bearing cross section that controls most of the properties [9-12], and measuring the conductivity in-situ would be an attractive method to follow the sintering process. However, $\boldsymbol{\kappa}$ is fairly difficult to measure in-situ mainly due to contacting problems at elevated temperatures, the contacts inevitably exhibiting temperature gradients that affect the resistivity of the system in a rather unpredictable way. As shown by Simchi et al., the change of conductivity is most pronounced in the early stages of sintering while especially in the later stages of isothermal sintering, changes are marginal [10-12]. Therefore, characterization of electrical (or thermal) conductivity seems to be particularly suited for the heating section of the sintering cycle which however, as stressed by Schatt [13], is of high relevance for the entire sintering process.

For metallic materials, $\boldsymbol{\kappa}$ is linked to the thermal conductivity $\boldsymbol{\lambda}$ through Wiedemann-Franz' law, i.e.

$$\lambda/\kappa = k.T \qquad (1)$$

k being a constant of about 2.44E-8 $V^2.K^{-2}$ [14]. I.e. measuring the thermal conductivity should give information about the microstructural changes as well as measuring the electrical conductivity.

Measuring the thermal conductivity in situ at elevated temperatures is also tricky, but the thermal diffusivity $\boldsymbol{a}$ – which is linked to $\boldsymbol{\lambda}$ by the relationship

$$\boldsymbol{a} = \lambda/\rho.c_p \qquad (2)$$

can be more easily measured using modern equipment, and measurement of c_p is routine in thermal analysis now, as is the change of the density with temperature through dilatometry.

Today, determination of the thermal diffusivity through the laser flash method is a quite mature technique and can be regarded as a reliable tool for standard materials. It has been applied e.g. for studying the sintering of ceramics, in part combined with other thermoanalytical methods [15]. In this case, sintering is linked to pronounced densification, typically full density being targeted with high performance ceramic materials. On the other hand, it could not be taken for granted that laser flash can be properly used also for porous metal bodies that markedly change their microstructure during sintering – i.e. also during the measuring routine – but not so much their total porosity, as characteristic for sintered steels used for PM precision parts,.

In the present study, in-situ sintering of compacts prepared from plain iron, Fe-C as well as Mo and Cr-Mo prealloy steels has been studied using the laser flash technique. Prealloyed powders were used to avoid effects of alloy element homogenization [16, 17] which would also affect the conductivity (see e.g. [18]). The sintering behaviour of these materials had already been studied in detail through conventional techniques, using e.g. interrupted sintering runs with subsequent characterization of the specimens [19-21]. The reliability of the laser flash measurements could thus at least qualitatively be checked.

EXPERIMENTAL PROCEDURE AND MATERIALS

Powder compacts were prepared from water atomized powders, iron powder ASC 100.29 and prealloyed steel powders Astaloy Mo and Astaloy CrM being used (all supplied by Höganäs AB, Sweden). In part natural graphite (Kropfmühl UF4) was admixed. The compositions tested are given in Table 1. The powder batches were mixed in a tumbling mixer (except for the plain iron powder) and uniaxially compacted to form billets with 16 mm diameter and about 5 mm thickness. The compacting pressure was set at 500 MPa, and die wall lubrication was afforded using Multical sizing fluid. The samples were pressed with a diameter significantly larger than the diameter of the sample holder (12.6 mm) to compensate for (improbable but possible) geometrical changes of the specimens by shrinkage during sintering.

Tab.1. Characteristics of the powder compacts used for in-situ measurements.

Code	Starting powder	$C_{nominal}$ [mass %]	Cr [mass %]	Mo [mass %]	Fe	Green density [$g.cm^{-3}$]
#1	ASC 100.29	-	-	-	Balance	6.97
#2	ASC 100.29	0.8	-	-	Balance	6.88
#3	Astaloy1.5Mo	0.8	-	1.5	Balance	6.89
#4	AstaloyCrM	0.8	3.0	0.5	Balance	6.71

The thermal diffusivity was measured using a laser flash apparatus Netzsch LFA 427 supplied by Netzsch Geraetebau GmbH (Selb, Germany). This equipment uses an Nd-YAG-Laser (pulse duration 0.5 ms; the temperature increase by the laser pulse is < 2 K). Details of the measuring technique are described in [22, 23].

The specimens were inserted into the vacuum chamber of the laser flash tester, and then the chamber was evacuated to a pressure of $<10^{-3}$ mbar. Since the laser flash apparatus requires stable thermal conditions, heating of the specimens had to be done stepwise. At each selected temperature, three parallel measurements of the thermal diffusivity were done while holding the temperature of the sample constant. After the three shots, the sample was heated up to the next selected temperature with a heating rate of 10 K/min. The whole procedure can be characterized by an average heating or cooling rate of about 3 K/min. Each run was done in a heating and cooling ramp, and a second (parallel) run was performed immediately after the first one, in order to study the microstructural changes caused by the first thermal cycle. The maximum temperature was set at 1000°C for both the first and the second cycle.

At temperatures above 200°C, the uncertainty of measurement regarding the values of thermal diffusivity is less than 5 %. At lower temperatures larger uncertainties exist because of a reduced sensitivity of the infrared detector. The temperature uncertainty is about 5 K (heating) ... 10 K (cooling).

The specific heat capacity c_p was measured by standard DSC technique calibrated with sapphire standards. Pressed samples were investigated in a heat flux DSC 404 supplied

by Netzsch Gerätebau GmbH (Selb / Germany). The measurements were done in high purity argon (99.999%) with a heating rate of 20 K/min. The uncertainty of measurement regarding the values of specific heat capacity is less than 10 %. The temperature uncertainty is about 1 K.

In Figure 1 the microstructures of the materials investigated are shown; to simulate the state of the laser flash specimens after the runs, impact test bars were prepared at the same conditions, i.e. pressed at 500 MPa and sintered following the same cycle; as atmosphere, the high purity air was used. As can be seen, the microstructures are fairly coarse, which is evident both with plain Fe and the carbon containing steels and is not surprising due to the very slow cooling. In the case of plain Fe, coarsening is further enhanced by the transformation effect described e.g. in [24, 25]. Furthermore, the fraction of ferrite is rather high considering the carbon content, which is particularly noticeable with Fe-0.8%C; also this can be attributed to the slow cooling which enhances formation of ferrite. Of course also some carbon loss must be considered occurring by reaction with the natural oxygen content of the metal powders.

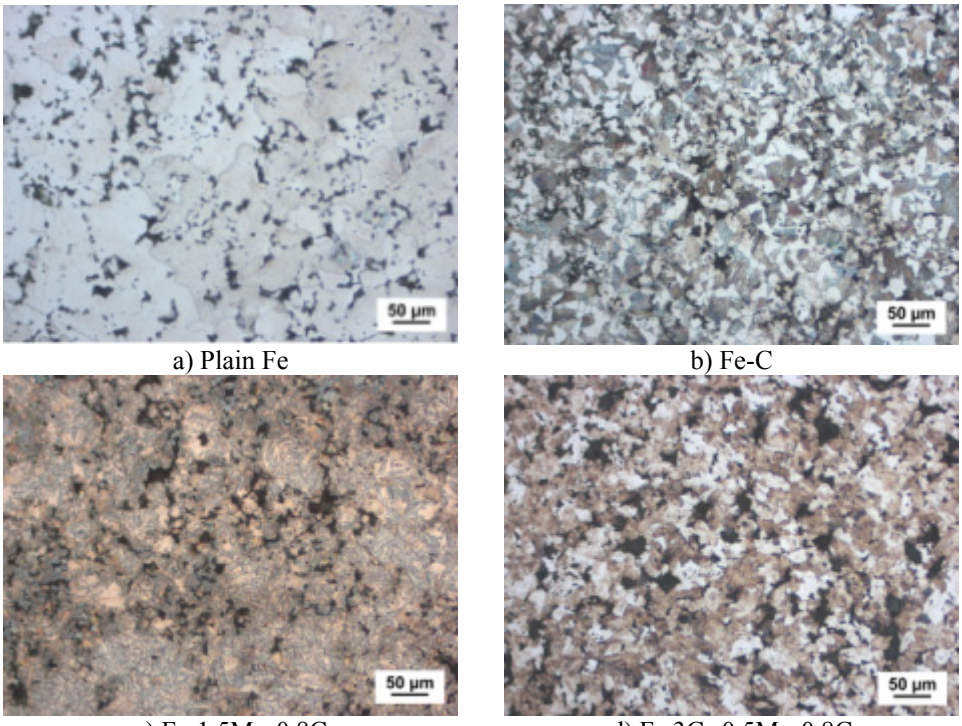

a) Plain Fe b) Fe-C

c) Fe-1.5Mo-0.8C d) Fe.3Cr-0.5Mo-0.8C

Fig.1. Microstructures of powder compacts sintered in Ar following the same sintering profile as in the laser flash device.

EXPERIMENTAL RESULTS – IN-SITU LASER FLASH TESTS

The thermal diffusivity data obtained for plain iron are given in Fig.2 as a function of the temperature for the first (Fig.2a) and the second run (Fig.2b). Parallel runs with other specimens yielded virtually identical results, which indicates that the reproducibility of the method is highly satisfactory. As can be clearly seen there are considerable differences

between the heating and cooling sections in the first run while in the second run the results for heating and cooling are virtually identical. This confirms that those changes of the microstructure that are relevant for affecting the thermal diffusivity occur virtually exclusively during the first heating stage; after this stage the microstructural changes do not have any noticeable effect on the thermal diffusivity (at least unless the maximum temperature of the first run is not exceeded in the second run). This indicates that the processes influencing the thermal diffusivity are predominantly temperature-controlled (as are also e.g. the degassing phenomena in sintered steels, see [20, 26]). This further implies that the stepwise heating mode that is necessary for the laser flash experiments should not yield markedly different results from those that would be obtained in case of continuous heating with the same integral heating rate.

From the comparison of the heating and cooling stages in the first run it is further clear that the primary differences are found in the low temperature range, i.e. below approx. 600°C, which agrees well with the results given by Simchi et al. for the electrical conductivity [10, 11]. Generally the changes of the thermal diffusivity are not too pronounced, both with regard to the temperature effect – the spread here being from 0.04 to 0.21 $cm^2.s^{-1}$ maximum – and from the material, the differences between the green compact and that after the second run being in the range of less than 1:2 which indicates that in green compacts pressed with die wall lubrication the thermal diffusivity – and also the conductivity – is not too low, which also agrees with the findings of Simchi et al. for the electrical conductivity [10, 11] who found that for die wall lubricated compacts the increase of the conductivity is less pronounced than for compacts with admixed lubricants since also the initial level, i.e. $\boldsymbol{\kappa}$ of the compacts, is much higher in the former case, due to the absence of insulating organic substances in the pressing contacts.

Addition of carbon to the metal powders results in a further component the particles of which are located especially in the pressing contacts of the green compact (and of course also in the pores, which however should not be of much effect here). The respective graphs thermal diffusivity vs. temperature for the plain carbon steel Fe-0.8%C are given in Fig.3. Here it stands out quite clearly that the differences between the graphs for the heating and cooling sections, respectively, are markedly more pronounced than in the case of the plain iron compacts (Fig.2a). In particular the low temperature section of the heating graphs exhibits markedly lower $\boldsymbol{a}$ values. This may be attributed to the fact that graphite is less conducting (both for heat and electricity) than is metal, and the graphite flakes enclosed in the pressing contacts thus exert an effect on the conductivity that is more pronounced than that of the very thin oxide layers covering the iron particles, which furthermore are to some extent penetrated during pressing.

On the other hand, the decrease of $\boldsymbol{a}$ in the temperature range RT .. 400°C which is particularly pronounced in the case of the plain iron (from 0.12 to 0.04 $cm^2.s^{-1}$) is much smaller with the Fe-C compact with regard both to the absolute and the relative drop of the thermal diffusivity. Since the drop in the thermal diffusivity of the matrix metal should be the same for plain iron and iron-carbon (the graphite not yet being dissolved in the latter) it must be concluded that there is a relative improvement in the "quality" of the contacts, and here it can be assumed that the cleaning of the particle surfaces due to desorption of adsorbed gases and the decomposition of hydroxides is more pronounced in the case of graphite containing materials since it has been shown that apparently a considerable fraction of the compounds that are removed in the first part of the sintering process (up to about 400°C) originates from the graphite (see [26]). This cleaning of the surface results in an increased thermal diffusivity which in part compensates for the drop of $\boldsymbol{a}$ in the base metal.

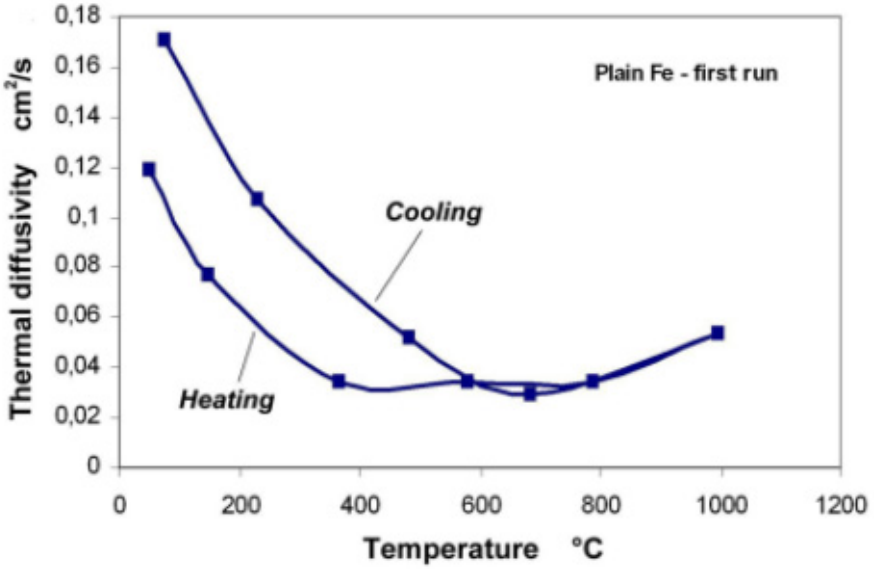

a) First run

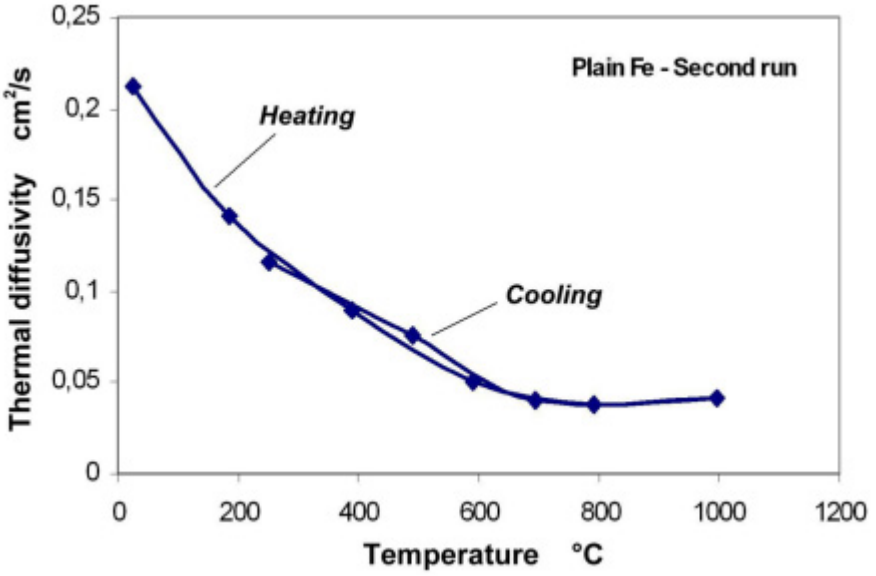

b) Second run

Fig.2. Thermal diffusivity of plain iron as a function of the temperature during a sintering run up to 1000°C. Atomized iron powder, compacted at 500 MPa, vacuum.

The cooling graph shows the same trend as that of plain iron, indicating that this behaviour is controlled by the behaviour of the matrix material, although the level of ***a*** remains lower (due to the different, i.e. two-phase microstructure). Also here, as in the case of plain iron, no effect of the α-γ phase transformation – which for Fe-C occurs at significantly lower temperatures than for Fe - is discernible in the graphs.

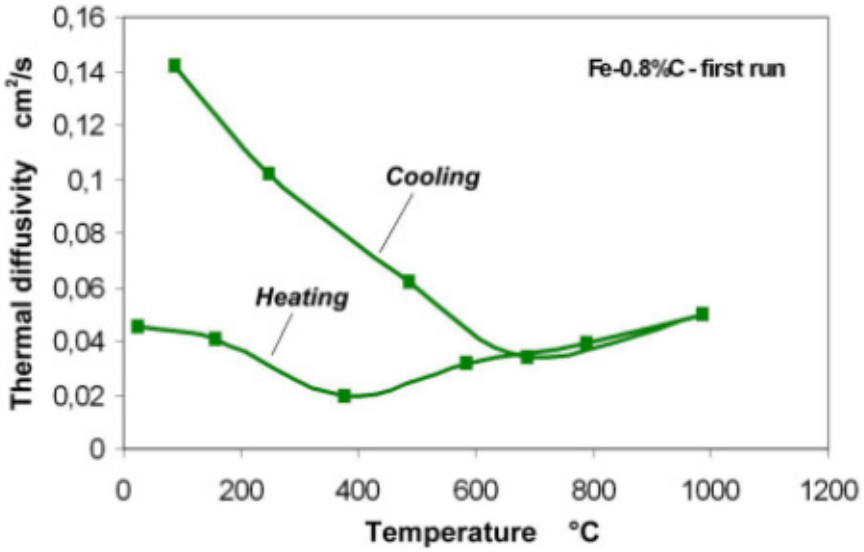

Fig.3. Thermal diffusivity of Fe-0.8%C as a function of the temperature during a sintering run up to 1000°C. Atomized iron powder, compacted at 500 MPa, vacuum.

As stated above, the alloy steels containing Mo and Cr-Mo, respectively, were prepared from prealloyed powders, and therefore no homogenisation effects – except of course of carbon – should occur. The graphs are shown in Fig.4. Here it stands out clearly that the trend is quite similar to that observed with the Fe-C material, i.e. compared to plain iron a rather low initial value for the thermal diffusivity but also a rather slight drop towards higher temperatures.

A typical feature is the fact that with both materials the virtual overlap of the heating and cooling graphs in the temperature range 600…1000°C is not discernible any more but that the increase of ***a*** in the heating section is more pronounced than the decrease in the cooling branch. This effect is particularly characteristic for the higher alloyed steel Fe-3%Cr-0.5%Mo-C but can be seen to some extent also with Fe-1.5%Mo-C. The Cr alloy steel however does not exhibit the typical steady increase of ***a*** between 600 and 1000°C but there is only one large step between 800 and 1000°C. Here it must be kept in mind that according to Kremel et al. [19], reduction of the oxide layers covering the Fe-Cr-Mo prealloy particles takes place only at about 1000°C minimum while for Fe-C or also Fe-Mo-C this effect occurs at about 700 ... 800°C. As shown in [27], formation of stable sintering necks is possible only after the reduction process has occurred. Therefore it can be assumed that for the Cr-Mo steel the carbothermal reduction of the oxides at the maximum temperature of the measuring run has resulted in neck formation and an according increase of the thermal diffusivity while with the other steels the deoxidation occurs at much lower temperatures, and neck formation is thus governed rather by the onset of diffusion and not by a chemical reaction.

The cooling branches of the respective graphs are quite similar to those found in Fe and Fe-C; of course the absolute levels for the ***a*** values are again lower due to the effect of the dissolved alloy elements. However, this effect becomes more pronounced at lower temperatures, which agrees with the results described in [26] which showed that the effect of solid solution on the thermal conductivity decreases with higher temperatures and virtually disappears at T > 600°C while that of the porosity remains.

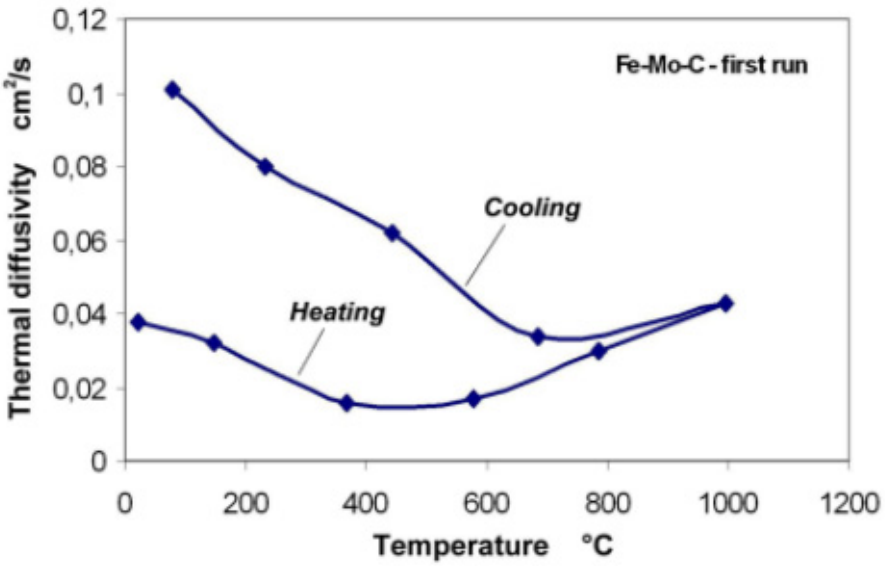

a) Fe-1.5%Mo-0.8%C

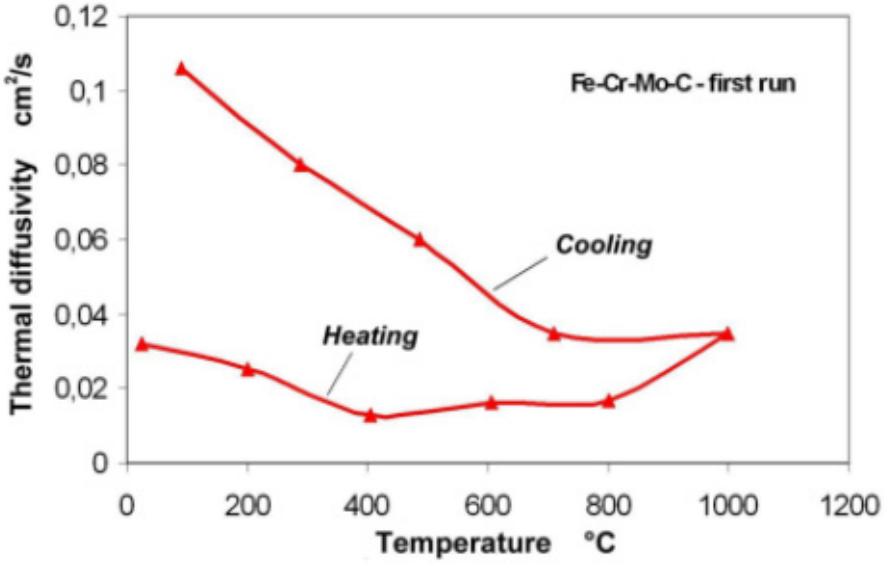

b) Fe3.0%Cr-0.5%Mo-0.8%C

Fig.4 Thermal diffusivity of alloy steels Fe-1.5%Mo-0.8%C and Fe-3%Cr-0.5%Mo-0.8%C as a function of the temperature during a sintering run up to 1000°C. Atomized prealloyed iron powder, compacted at 500 MPa, vacuum.

DISCUSSION

Thermal diffusivity measurements for in-situ characterization of the sintering process have been successfully used with cemented carbides. However, the sintering behaviour of PM ferrous compacts differs markedly from that of hardmetals (WC-Co, ...).

The latter are characterized by a pronounced densification during sintering, indicated by accordingly high shrinkage of typically 16 ... 18 % linear (similar to sintering of ceramics, see above). Shrinkage begins when oxidic impurities on the surfaces of the hard material particles (WC, ...) are reduced by the carbon of the mixture [29]. Only above these temperatures shrinkage takes place, caused by diffusion processes. Due to the same reasons the contact areas between the particles are cleaned and enlarged, and thus a better heat transfer through the porous sample is possible. In [30] it has been shown that a pronounced increase of thermal diffusivity and a similarly pronounced decrease of length coincide, starting at a temperature of 750 °C for a standard grain size hard metal WC-10 wt.% Co (DS 130 from HC Starck / Germany).

With ferrous PM compacts, on the other hand, the role of densification is rather marginal, and the improvement of the mechanical properties during sintering is almost exclusively due to changes in neck – i.e. in sintering contact – geometry while the total porosity remains practically unchanged. This results in much lower effect of sintering on thermal and mechanical properties, and it might therefore be assumed that the thermal conductivity/diffusivity is decidedly better suited for characterizing the sintering process of specimens the porosity of which changes drastically during sintering – hard metals, heavy alloys, MIM products – than sintering of ferrous parts.

However, also for the latter of course the increase in neck dimension and strength has some impact on the electrical and thermal properties. As shown quite early by Esper et al. [6], and later in more detail e.g. by Simchi [10-12] for the electrical conductivity, the effect of sintering is most pronounced in the early stages of the sintering process while e.g. a change of the sintering temperature from 1120° to 1250°C has only marginal effect on $\boldsymbol{\kappa}$.

The same phenomenon seems to hold also for the thermal properties, which is not surprising due to the close links between thermal and electrical conductivity of metallic materials. In order to assess if the results for $\boldsymbol{a}$ obtained in-situ through laser flash are in agreement with the conductivity/resistivity values obtained with the same type of materials by Simchi et al. [10-12], first the thermal conductivity $\boldsymbol{\lambda}$ was calculated according to Eq.2 from the $\boldsymbol{a}$ values obtained for plain iron. The density values for the various temperatures were taken from the literature [31] as were the values for the specific heat c_p [29, 30]; experimental measurements (see above) were found to be in good agreement with the literature data. As a reference, the data for fully dense plain iron were taken. The resulting values are given in Fig.5; also the relative thermal conductivity, i.e. that of the porous body normalized to that of fully dense material at the same temperature, is plotted there.

The striking similarity between the graphs for the porous and the dense materials and those plotted in Fig.1a is quite evident which indicates that in fact during the *cooling section* of the test run the thermal properties of the material are affected primarily by the matrix material rather than by changes of the pore structure or neck characteristics. In the *heating section*, on the other hand, the latter mechanisms seem to play a major role. The drop in the relative thermal conductivity between RT and 400°C is at first surprising, at least when taking into account the behaviour of the carbon containing steels in this temperature range (Fig.3); however it reflects the more pronounced drop of $\boldsymbol{a}$ in this temperature range observed with plain iron. One possible explanation might be that in plain iron there are no graphite particles which, though they are rather poor conductors, form bridges in the pressing contacts while in plain iron the removal of the volatile surface compounds – which are electrically insulating but nevertheless thermally conducting - tends to weaken the pressing contacts until the onset of sintering results in the formation of more stable bridges (see discussion below). In any case it is clearly evident that the main increase

of the relative conductivity occurs between 500 and 800°C, at least qualitatively quite similar to the effects of sintering reported for the electrical conductivity.

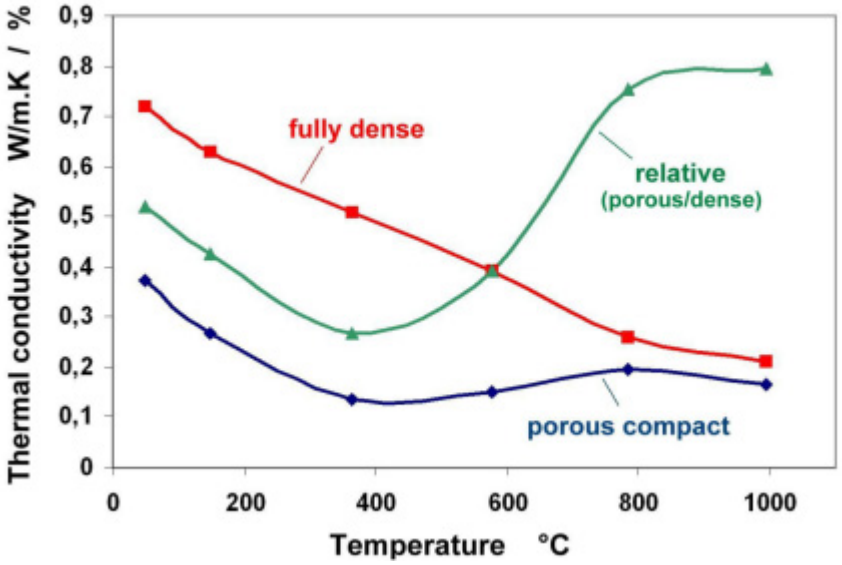

Fig.5. Thermal conductivity λ (calculated from a obtained through laser flash) of a porous plain iron compact (first heating) compared to the theoretical values for a fully dense body.

If the electrical resistivity of the plain iron specimens is calculated from the thermal conductivity using Wiedemann-Franz' law (Eq.1) the graphs given in Fig.6 are obtained. Due to the direct relationship the graph is virtually a reverse plot of that given in Fig.5 (though somewhat distorted by the effect of the temperature). For comparison, the resistivity of fully dense plain iron is also given. The almost parallel trend of the graphs of the cooling section and of the theoretical values for fully dense iron is evident, once more confirming that all changes of the pore structure and neck geometry have occurred in the heating section while during cooling only the resistivity of the matrix metal is of importance.

If the results obtained are compared to those given by Simchi et al. [10, 11] it stands out clearly that the initial resistivity, i.e. that of the green compact, calculated from laser flash data is much too low, being in the range of about 0.2×10^{-4} Ω.cm while Simchi gives values of $>50 \times 10^{-4}$ Ω.m for the green compact (pressed with die wall lubrication). On the other hand, after the cooling run the final resistivity is in very good agreement with Simchi's values, being in the range of about 0.15×10^{-4} Ω.m, while Simchi gives about 0.13×10^{-4} Ω.m.

This discrepancy can be explained by the fact that Wiedemann-Franz' law holds for metallic systems while initially the powder particles surfaces are covered by oxides, hydroxides, in part also lubricant, for which this correlation between electrical and thermal properties cannot be applied, the non-metallic layers being thermally conductive but not electrically, and calculating the electrical conductivity κ from the thermal one gives too high κ = too low resistivity. Only at a temperature at which the non-metallic layers have been removed to a considerable extent, i.e. when the metallic contacts dominate the

interfacial area between the powder particles, thermal and electrical conductivity tend to agree.

This means that if in-situ methods are to be used for assessing the formation and growth of metallic contacts, determination of the resistivity is better suited than that of the thermal conductivity / diffusivity since the latter is contributed to also by insulating layers that do not bear any load. On the other hand, measuring the thermal diffusivity through laser flash is fairly easy and not as sensitive to experimental problems while yielding quite interesting results at least for the low to moderate temperature range of sintering. At higher temperatures the heat transfer by radiation must be taken into account which takes place also through the pore space, and the role of the sintering contacts will probably be somewhat obscured.

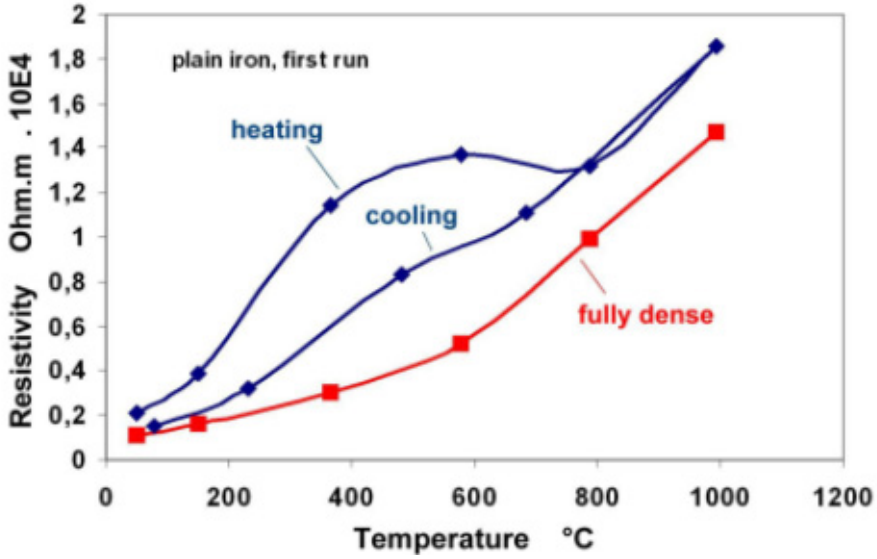

Fig.6. Resistivity of plain iron, calculated from the thermal diffusivity (first run, heating and cooling), as a function of the temperature.

When comparing the evolution of thermal diffusivity for the different materials investigated here, it is helpful to compare on one hand the heating section and on the other hand the cooling part separately. In Fig.7a, the heating section is shown for Fe and Fe-0.8%C. It is evident that, as stated above, at low temperatures, i.e. for the pressed compact, there is a pronouncedly lower diffusivity for the Fe-C specimen compared to Fe; however, the drop of ***a*** with higher temperatures is markedly less pronounced. At about 600°C the two graphs virtually merge, which is somewhat surprising insofar as it excludes graphite as the main reason for the lower ***a*** of the Fe-C materials: as shown e.g. in [20, 33], graphite is dissolved to a considerable degree only well above 800°C. It seems that the dissolution of graphite plays a much lower role towards the thermal diffusivity than the formation of the first metallic bridges. This is also evident from the fact that in the temperature range 800 …1000°C there is hardly any difference between Fe and Fe-C; if graphite played a major role, a significant change of a would be noticeable in the dissolution range 800 … 1000°C. It can be assumed that volatile compounds introduced with graphite are more effective towards ***a*** than the graphite itself, which is rather well conducting.

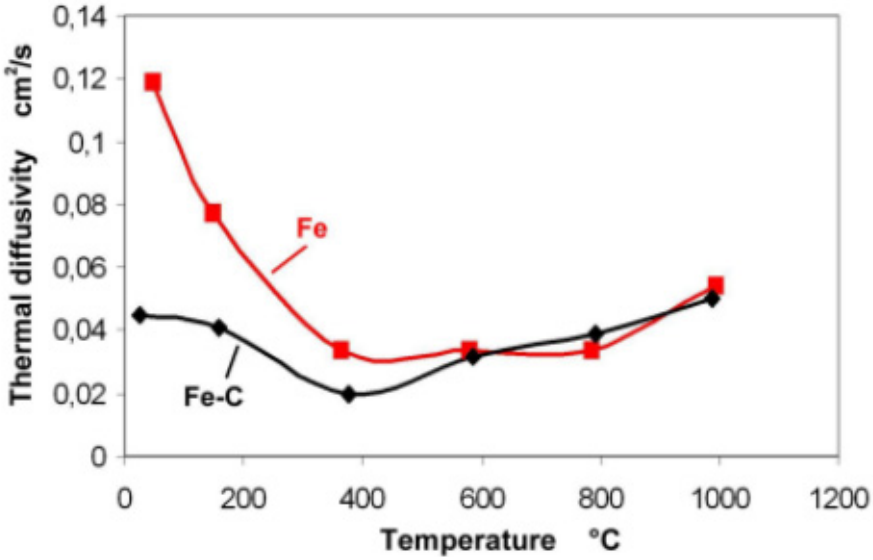

a) Heating section

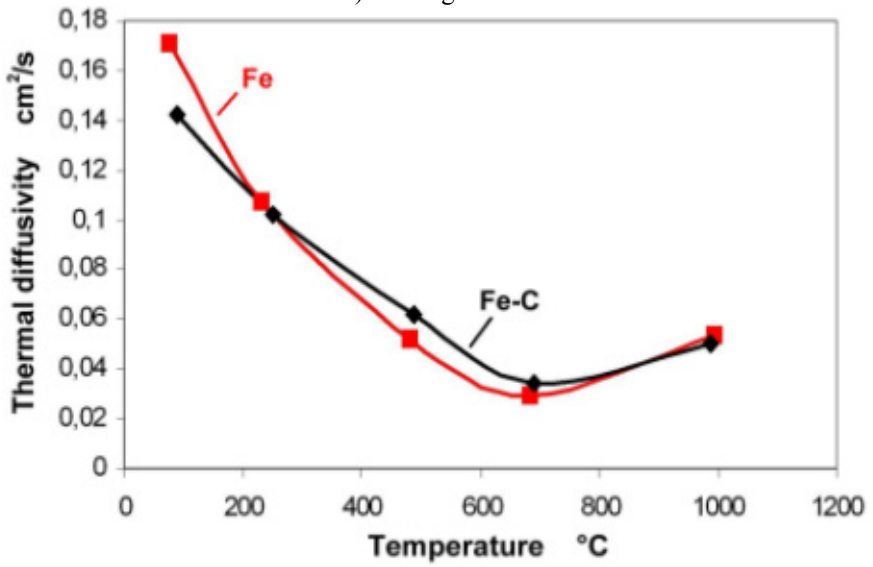

b) Cooling section

Fig.7. In-situ thermal diffusivity of Fe and Fe-0.8%C as a function of the temperature during a sintering run up to 1000°C.

From the cooling sections (Fig.7b) can be concluded that the effect both of dissolved carbon (in the austenite range) and of cementite on the thermal diffusivity is rather minor since both graphs coincide; only close to room temperature the plain iron material shows a slightly better ***a*** value. This agrees with the findings shown in [28] that at higher temperatures the porosity rather than the alloy elements affect thermal and electrical conductivity. In any case, the transport capacity of the sintering contacts for heat seems to be very similar for both materials. Here it should be considered that while the conductivity

of the matrix might be slightly lowered by the presence of carbon (dissolved or as Fe_3C) the effect of sintering will be somewhat more pronounced in Fe-C since the maximum sintering temperature applied here (1000°C = 1273 K) is 70% of the absolute solidus temperature for Fe compared to 77% for Fe-C, i.e. for Fe-C the sintering effect will be slightly more pronounced.

Including also the alloyed steels in the comparison (Fig.8) confirms that at room temperature it is mostly the graphite that influences the thermal diffusivity; in the heating section the graphs for Fe-Mo-C and Fe-Cr-Mo-C show a very similar behavior as Fe-C, just at a slightly lower level. At temperatures >600°C the Cr-Mo prealloyed steel differs from the other materials insofar as the increase of the diffusivity starts at 800°C compared to 600°C for the others, which, as stated already above, is an indicator of the stable surface oxides covering the Cr prealloyed powders. As shown e.g. in [34] it is the temperature range between 400 and 600°C within which the thin iron oxide layers initially covering the Cr-Mo steel powders [35] are transformed into more stable oxides than inhibit sintering ("internal getter" effect). Not the stable oxides themselves (which are still very thin) but their adverse effect on sintering is responsible for the slower increase of ***a*** with this material. For this type of steel, 1000°C is rather a low sintering temperature anyhow since the oxide layers just start to be carbothermally reduced [21], which explains why the a value for Fe-Cr-Mo-C recorded at 1000°C is lower than for the other steel grades.

The cooling section, in contrast, shows that this difference is virtually eliminated during cooling; at about 700°C rather identical thermal diffusivity values are measured for all the materials tested here. Only below 400°C the effect of the alloy elements becomes noticeable, the graphs for the alloyed steels deviating from those for Fe and Fe-C. This once more confirms that the effect of alloying elements on thermal diffusivity and conductivity is quite pronounced at and near room temperature but tends to virtually disappear at higher temperatures [28].

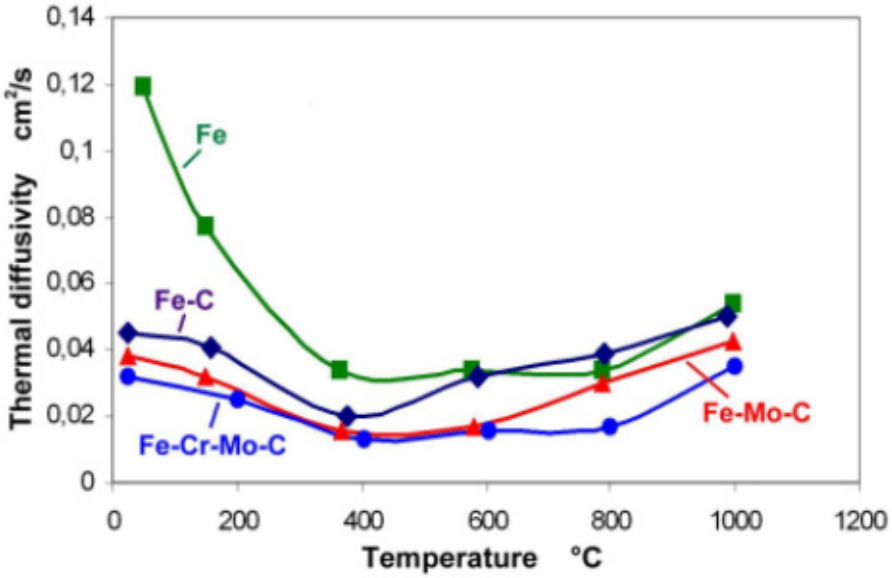

a) Heating section

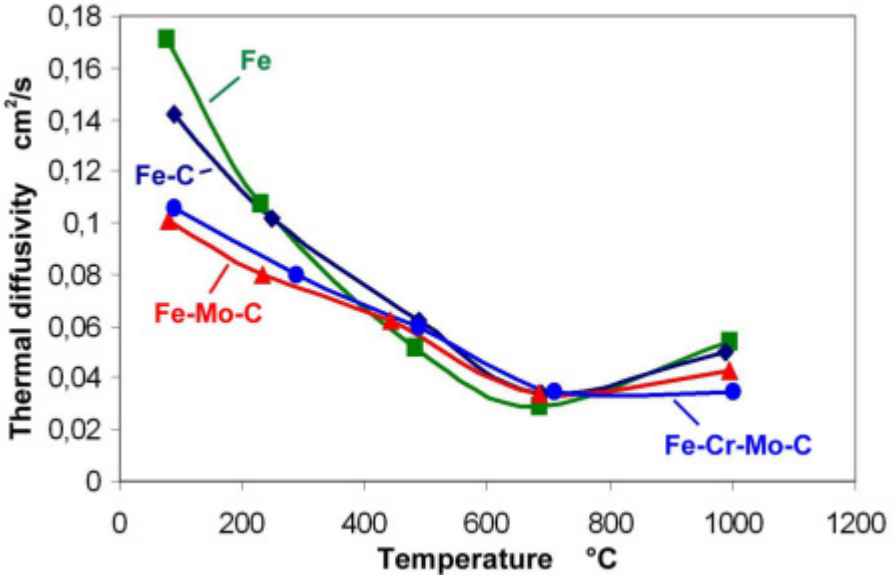

b) Cooling section

Fig.8. In-situ thermal diffusivity of different ferrous powder compacts as a function of the temperature during a sintering run up to 1000°C.

CONCLUSIONS

- In-situ measurement of the thermal diffusivity ***a*** during a simulated sintering run can be done by using the laser flash method. If the tests are done in vacuum, also porous powder compacts can be measured without undesirable interaction with the atmosphere.
- By carrying out test runs with plain iron compacts up to 1000°C it could be shown that the main changes occurring in the material that noticeably affect ***a*** occur at rather low temperatures, as evident when comparing the heating and the cooling sections. The cooling run yields virtually the same graph as does the second run in both heating and cooling. This indicates that the relevant processes are virtually temperature controlled, and the stepwise heating necessary with laser flash tests should not affect the results compared to constant heating rates.
- Carbon added as graphite results in lower initial diffusivity but on the other hand in a lower drop of ***a*** during heating. This can be attributed to the poor thermal conductivity of graphite compared to metal but on the other hand to the beneficial removal of volatile compounds in the early sintering stages.
- Alloy steels prepared from prealloyed powders result in quite similar heating graphs as does Fe-C, however the ***a*** levels are slightly lower. Esp. with Cr alloyed material the increase of ***a*** commonly observed in the temperature range 600…1000°C takes place only closely below the maximum temperature, i.e. above 800°C, indicating that the higher temperatures necessary for surface reduction in this material affect the formation of sintering contacts.
- In the cooling sections the materials differ only insignificanrly down to about 400°C; below this temperature the alloy steels show progressively lower ***a*** with decreasing temperature while the graphs for Fe and Fe-C separate only below 200°C, indicating

that the effect of C – as cementite – is less pronounced than that of metallic alloy elements such as Cr or Mo.

- Generally, the change of a during sintering is markedly less pronounced with ferrous compacts than with e.g. hard metals, due to the much lower change of the total porosity which in hard metals virtually disappears while in ferrous compacts it is only marginally reduced.
- From the values for the thermal diffusivity the thermal conductivity λ can be calculated which in turn can be used to calculate the electrical resistivity κ using Wiedemann-Franz' law for the λ-κ relationship. If this is done and the results are compared with resistivity data from previous investigations it is found that at least for plain iron the initial resistivity, i.e. that calculated from the green compact, is much too low while the final one, after the test run, is in excellent agreement with the experimentally obtained resistivity values. This indicates that in the initial stage the particle contacts are predominantly non-metallic, and thus Wiedemann-Franz' law cannot be applied, while after the test run metallic contacts are present for which the λ-κ relationship can be successfully used.

REFERENCES

[1] German, RM.: Int. J. Powder Metall., vol. 38, 2002, no. 2, p. 48
[2] Schatt, W: Sintervorgänge. Düsseldorf : VDI-Verlag, (1992
[3] Leitner, G., Jaenicke-Roessler, K., Gestrich, T., Breuning, T.: Metal Powder Report, vol. 52, 1999, no. 12, p. 32
[4] Gierl-Mayer, C., Danninger, H.: Powder Metall. Progress, vol. 15, 2015, no. 1, p. 3
[5] Shoales, GA.: P/M Sci. & Technol. Briefs, vol. 3, 2001, no. 1, p. 18
[6] Mousapour, M., Azadbeh, M., Danninger, H.: Powder Metallurgy, vol. 59**,** 2016, no. 5, p. 321
[7] Esper, FJ., Exner, HE., Metzler, H.: Powder Metall., vol. 18, 1975, p. 107
[8] Fortschritte der Pulvermetallurgie. Eds. F. Eisenkolb, F. Thümmler. Bd. 1. Berlin : Akademie-Verlag, 1963, p. 387
[9] Cytermann, R.: Powder Metall. Int., vol. 19, 1987, no. 1, p. 27
[10] Simchi, A., Danninger, H.: Powder Metall., vol. 43**,** 2000, no. 3, p. 209
[11] Simchi, A., Danninger, H., Weiss, B.: Powder Metall., vol. 43**,** 2000, no. 3, p. 219
[12] Simchi, A., Danninger, H., Gierl, C.: Powder Metall., vol. 44**,** 2001, no. 2, p. 148
[13] Schatt, W.: Powder Metall. Int., vol. 18, 1986, no. 1, p. 45
[14] Westphal, WH.: *Physik*, Springer-Verlag, Berlin-Göttingen-Heidelberg, 1959, p.314
[15] Raether, F., Springer, R.: Adv. Eng. Mater., vol. 2, 2000, no. 11, p. 741
[16] Danninger, H.: P/M Science & Technol. Briefs, vol. 1, 1999, no. 5, p. 19
[17] Danninger, H., Gierl, C., Leitner, G. In: Proc. 2000 Powder Metall. World Congress, Kyoto. Eds. K. Kosuge, H. Nagai. Part 2. The Japan Soc. of Powder and Powder Metall, 2001, p. 943
[18] Jangg, G., Drozda, M., Danninger, H., Schatt, W., Wibbeler, H.: Int. J. Powder Met. & Powder Techn., vol. 20, 1984, p. 287
[19] Danninger, H., Wolfsgruber, E., Ratzi, R. In: Proc. PM98 Granada. Vol. 2. Shrewsbury : EPMA, 1998, p. 290
[20] Danninger, H., Gierl, C.: J. Mater. Chem. & Physics, vol. 67, 2001, p. 49
[21] Kremel, S., Danninger, H., Yu, Y.: Powder Metall. Progress, vol. 2, 2002, no. 4, p. 211
[22] Netzsch Geraetebau, LFA 427 Data Sheet, Selb, D-95088 Selb / Germany
[23] Perl, M., Leitner, G: J. Thermal Analysis, vol. 47, 1996, p. 643
[24] Lehr, P.: C.R.Acad.Sci.France, vol. 242, 1956, p. 1172

[25] Kuroki, H., Suzuki, HY.: Mater. Transactions, vol. 47, 2006, p. 2449
[26] Danninger, H., Kremel, S., Leitner, G., Jaenicke-Roessler, K., Y,u Y.: Powder Metall. Progress, vol. 2, 2002, no. 3, p. 125
[27] Kremel, S., Raab, C., Danninger, H. In: Proc. EuroPM2001 Nice. Vol. 1. Shrewsbury: EPMA, 2001, p. 52
[28] Danninger, H., Gierl, C., Mühlbauer, G., Silva Gonzalez, M., Schmidt, J., Specht, E.: Int. J. Powder Metall., vol. 47, 2011, no. 3, p. 31
[29] Gille, G., Leitner, G., Roebuck, B. In: Proc. Europ. Conf. Adv. Hard Metals Prod., Stockholm. Shrewsbury : EPMA, 1996, p. 195
[30] Leitner, G.: J. Thermal Analysis and Calorimetry, vol. 56, 1999, p. 455
[31] Handbuch der Sonderstahlkunde. Ed. Houdremont. 3rd ed. Springer, 1956
[32] Thermophyikalische Stoffgrößen. Ed. W. Blanke. Springer, 1989
[33] Danninger, H., Frauendienst, G., Streb, KD., Ratzi, R.: Mater. Chemistry & Physics, vol. 67, 2001, p. 72
[34] Gierl-Mayer, C., de Oro Calderon, R., Danninger, H.: JOM, vol. 68, 2016, no. 3, p. 920
[35] Karlsson, H., Nyborg, L., Berg, S., Yu, Y. In: Proc. EuroPM2001, Nice. Vol. 1. Shrewsbury : EPMA, 2001, p. 22

Appendix: List of symbols

a …… thermal diffusivity [$cm^2.s^{-1}$]
c_p ….. Specific heat, at constant pressure; [$J.mole^{-1}.K^{-1}$]
κ …… electrical conductivity [$\Omega^{-1}.m^{-1}$]
λ …… thermal conductivity [$W.m^{-1}.K^{-1}$]
ρ …… density [$g.cm^{-3}$]

Powder Metallurgy Progress, Vol.18 (2018), No.2, p.096-102
http://dx.doi.org/10.1515/pmp-2018-0010

INVESTIGATION ON FEEDSTOCK PREPARATION FOR MICRO-CEMENTED CARBIDE INJECTION MOLDING

Abdolali Fayyaz, Norhamidi Muhamad, Abu Bakar Sulong

Abstract

This research was focused on mixing of submicron cemented carbide (WC-Co-VC) powder and binder. WC-Co-VC powder particle size and morphology were analyzed by laser diffraction and field emission scanning electron microscopy. The WC-Co-VC powder was kneaded with a paraffin wax based binder system. Based on critical solid loading, the feedstock with different solid loadings between 49 to 51 vol.% was prepared. Finally, the flow behavior of different feedstocks was investigated. Morphology of powder revealed that the particles of powder are slightly agglomerated and irregular in shape. The result of mixing indicted that the torque value increases as the solid loading increase from 49 vol.% to 51 vol.%. The feedstock exhibited homogeneity and the powder particles are homogenously coated with binder. The feedstock with solid loading of 51 vol.% is sensitive to temperature and showed high viscosity values. The feedstock with solid loadings of 49 and 50 vol.% had good compatibility and flow characteristics.

Keywords: Micro-cemented carbide injection molding, Mixing, Feedstock

INTRODUCTION

Cemented Carbide is a hard metal included a binder metal such as Nickel (Ni), Cobalt (Co) or Iron (Fe) and carbide usually either tungsten carbide (WC), VC (Vanadium Carbide), Cr_3C_2 (Chromium Carbide) and TiC (Titanium Carbide). It presents high hardness, high compressive strength, suitable thermal conductivity, and retains its hardness values at high temperatures. These properties cause to wide application of cemented carbide as mining, machining, metal cutting, metal forming and mold making [1-3].

In the recent years, many attempts have been undertaken to use powder injection molding (PIM) process technology for the manufacturing of micro parts, as called micro-powder injection molding (micro-PIM). Micro-PIM is a process used to fabricate metal, ceramic and carbide components and has several advantages such as shape complexity, near net-shape capability and high performance. This process has gained attractive processing technology in micro system manufacturing [4,5].

Abdolali Fayyaz: Department of Materials Engineering, Science and Research Branch, Islamic Azad University, Tehran, Iran.
Norhamidi Muhamad, Abu Bakar Sulong: Department of Mechanical and Materials Engineering, Faculty of Engineering and Built Environment, Universiti Kebangsaan Malaysia, 43600 Bangi, Selangor, Malaysia.

Micro-PIM has high potential for manufacturing complex cemented carbide (WC-Co) micro parts without subsequent finishing processes as known micro-cemented carbide injection molding (micro-CCIM) [6,7]. The processing steps of micro-CCIMM included four main steps. The process begins with kneading fine WC-Co powders with a binder to form a feedstock. Then feedstock inject into the mold, as called green part. After that, the binder removes from green part in debinding stage. In the next step, debinded part sintered to obtain final part with high physical and mechanical properties [6,8]. The mixing of powder and binder require special considerations in the micro-PIM, as the fine powders typically are more prone to agglomerate. For preparing feedstock from fine powder, higher shear needs to be applied to obtain homogenize feedstock, as the uniformity of the feedstock influences the rheological properties of powder-binder mixture. The success of injection molding in the micro-PIM is highly dependent on flow characteristics of the feedstock. The binder systems should provide low viscosity of feedstock and ensure the fluidity of feedstock to fill the die cavity completely [9,10]. Evaluation of rheological properties of the feedstock is the simplest method for prediction of feedstock behavior during injection molding [11]. Therefore, the present research attempted to investigate the mixing process of fine WC-Co powder and binder. The homogeneity and rheological properties of the feedstock, that are critical character in micro-CCIM process, are also studied.

EXPERIMENTAL MATERIALS AND METHODS

A composition of submicron WC-10Co-0.8VC powder was prepared as powder mixture for the present study. This hardmetal composition normally utilized in the hardmetals industry for tools application such as precision drills in dental application. The VC was doped in the powder mixture as grain growth inhibitor. The paraffin wax (PW) based was selected as binder system. It included (PW), polyethylene (PE) and stearic acid (SA). The weight percentage ratio of PW:PE:SA was 65:30:5. The properties of selected binder systems are listed in Table 1.

Tab.1. Properties of binder system components.

Binders	Melting point (°C)	Decomposition range (°C)
PW	63	205–375
PE	125	425–495
SA	61	165–305

Mixing of WC-10Co-0.8VC powder and binder components were performed using a twin-screw Brabender mixer W50 EHT with a volume of chamber 55 cm^3 as shown in Fig.1. The mixing temperature was selected 140°C. This temperature was above the highest melting temperature of (125°C) and less than the lowest decomposition temperature (165°C) of the selected binder system components. Feedstock with solid loading between of 49 vol.% to 51 vol.% were prepared based on critical solid loading. Detailed information about critical solid loading is reported elsewhere [10].

Fig.1. Twin-screw Brabender mixer W50 EHT.

Average particle size and distribution of WC-10Co-0.8VC powder were measured by using Malvern Zetasizer nano zs particle size analyzer, based on laser scattering method. Morphology of the powder and feedstock were also investigated by using field emission scanning electron microscope (FE-SEM). The flow behavior of different powder-binder mixture was examined by using Shimadzu Capillary Rheometer CFT-500D.

RESULTS AND DISCUSSION

The Figure 2 indicates the microstructure of the WC-10Co-0.8VC powder. The powder exhibited an irregular and angular shape morphology and was agglomerated. The high agglomerated powder is not suitable for the PIM process. The irregular shaped particle lead injection molding more difficult compare to spherically shaped particle, because of the irregular particle cause to increase viscosity of feedstock [12].

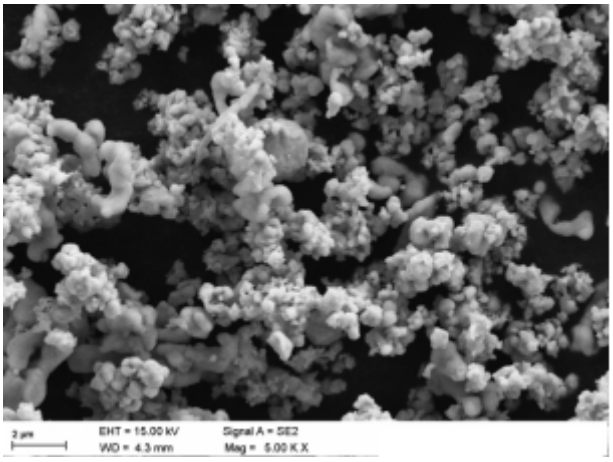

Fig.2. Microstructure of the WC-10Co-0.8VC powder.

The Figure 3 shows the distribution size of WC-10Co-0.8VC powder. The particle size analysis gave the distribution of WC-10Co-0.8VC powder, which presented D_{50} equal

to 0.67 μm. Previous study was reported using WC-10Co powder with a 0.5 μm particle size to manufacture small tools by PIM [13]. So, the particle size of powder in this study is fine enough to manufacture small WC-Co parts with high surface quality.

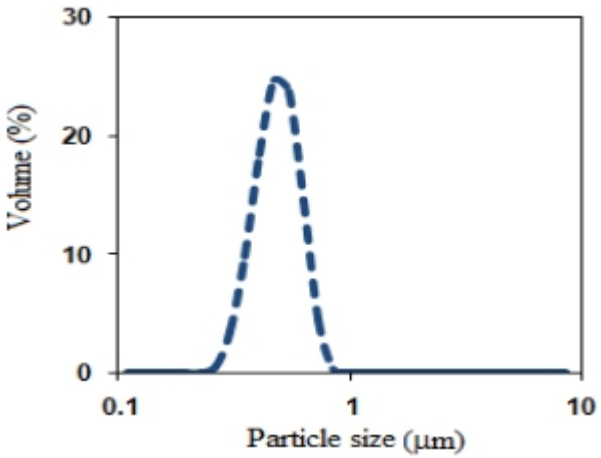

Fig.3. Particle size distribution of WC-10Co-0.8VC powder.

The preparation of feedstock that was performed through the kneading powder with binder is a critical process stage in PIM process, since the quality of feedstock influence on injection molding and debinding process. A proper mixed compound consists of a homogeneous powder which is dispersed among the binder.

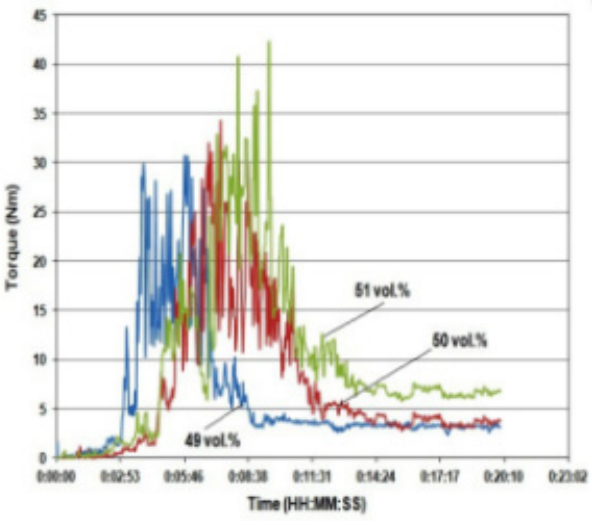

Fig.4. Torque variation versus mixing time of feedstock preparation different solid loadings.

The mixing torque, proportional to the shear stress of the mixer, indicates that the work energy consumed to disperse and distribute the powder in the binder [14]. Fig. 4

shows the variation of torque as a function of mixing time for different solid loadings of binder system. As it can be seen, the torque value increases as the solid loading increase from 49 vol.% to 51 vol.%. This is attributed to higher powder content require higher torque to wetting surface of powder particles. Fig. 4 also shows, the torque becomes stable in a short time that demonstrating uniform mixing in low solid loading. However, low solid loading has high tendency to powder and binder segregation during injection molding and also can cause to higher shrinkage after sintering [12]. For 51 vol.% solid loading, the torque value increased significantly with the mixing time. This shows that the powder was not uniformly distributed within the binder in short time, due to the binder could not fill completely the voids between the particles.

The ideal homogenous feedstock indicated low viscosity and any in-homogeneity in feedstock also affects the properties of molded, debinded and sintered parts [10]. The Figure 5 illustrates the micrograph of the final feedstock was prepared after mixing. The micrographs indicate that the powder particles were surrounded by binder components, which verifies that the powder-binder mixture is homogeneous. It also revealing to proper selection of kneading parameters due to mixed compound consists of a homogeneous powder which is dispersed among the binder.

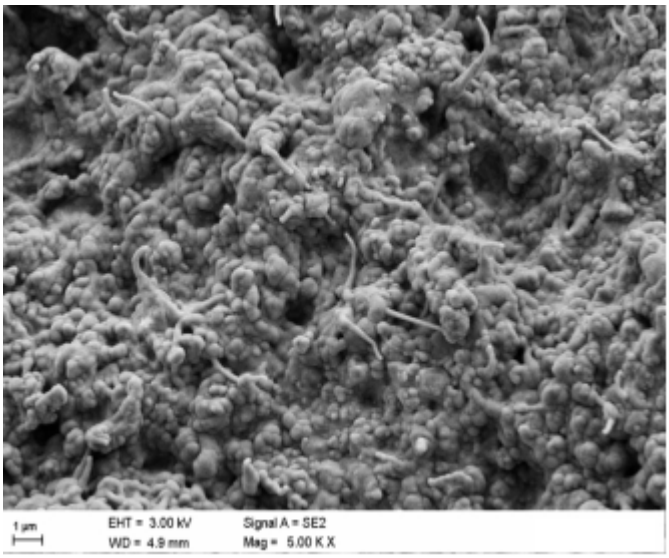

Fig.5. FESEM image of feedstock.

The success of the fabrication green part in the PIM is highly dependent on flow behavior of the powder-binder mixture. The binder systems should provide low viscosity of feedstock and ensure the fluidity of feedstock to fill the die cavity completely. The most important characteristics of the feedstock are its rheological properties, which relate mostly to viscosity [9]. Study of rheological properties is an important aspect for evaluation flowability of the feedstock. The variation of viscosity at different temperature in solid loading between 49 vol.% to 51 vol.% are presented in Table 2. The viscosity of feedstock decreases as the temperature increases. In this study viscosity of feedstock is very sensitive to temperature and when temperature increase, viscosity is low, especially at a high level of solid loading. As it found that the flow characteristics of feedstock with solid loading of 51

Vol.% is too much sensitive to temperature. The powder-binder mixture with solid loading 51 vol.% also indicated high viscosity at low temperature. Typically, the viscosity of a feedstock at the injection temperature should be in the range of 15-40 Pa.s for low pressure injection molding [15]. As can be seen from Table 2, the viscosity of feedstock with 49 vol.% and 50 vol.% solid loading indicate lower sensitivity to temperature. To compare the flow properties of different feedstocks, it indicates that the feedstock with solid loading 49 vol.% and 50 vol.% are within the suitable viscosity value for low pressure injection molding.

Tab.2.Viscosity at different temperature and solid loading.

Temperature (°C)	Viscosity [Pa.s] in different solid loading		
	42 vol.%	50 vol.%	51 vol.%
90	42	62	82
100	40	21	5
110	21	14	2

CONCLUSIONS

In the present work, the cemented carbide feedstock using submicron WC-10Co-V0.8C powder and the PW based binder system was produced for the micro-CCIM process of small components. The results show higher solid loading require higher torque to mixing powder and binder. The flow properties of the feedstock are used to predict the feedstock characteristics for fabricating micro part by micro-CCIM. The powder-binder mixture exhibited good homogeneity and the powder particles after mixing are surrounded with binder components. The feedstock with solid loading of 51 vol.% shows sensitivity to variation in temperature. It also found the powder-binder mixture shows high viscosity values at low temperature during the rheological test. The powder-binder mixture with solid loadings of 49 vol.% and 50 vol.% had good compatibility and flow characteristics. The lower solid loading also resulted in lower viscosity, therefore it is expected that injection process can carry out at lower temperature and fabricate green parts without any defects.

ACKNOWLEDGMENT

The authors would like to appreciate the Universiti Kebangsaan Malaysia (National University of Malaysia-UKM) for the support under the Grant No. DIP-2014-006 and UKM–ICONIC-2013-003.

REFERENCES

[1] Prakash, LJ.: International Journal of Refractory Metals and Hard Materials, vol. 13, 1995, no. 5, p. 257
[2] Fang, ZZ., Wang, X., Ryu, T., Hwang, KS., Sohn, H.: International Journal of Refractory Metals and Hard Materials, vol. 27, 2009, no. 2, p. 288
[3] Bose, A.: International Journal of Powder Metallurgy, vol. 47, 2011, no. 2, p. 31
[4] Attia, UM., Alcock, JR.: Journal of Micromechanics and Microengineering, vol. 21, 2011, no. 4, 043001
[5] Piotter, V., Bauer, W., Knitter, R., Mueller, M., Mueller, T., Plewa, K.: Microsystem Technologies, vol. 14, 2011, no. 251, p. 1
[6] Merz, L., Rath, S., Zeep, B.: Powder Injection Moulding International, vol. 1, 2007, no. 3, p. 56
[7] Heng, SY., Muhamad, N., Sulong, AB., Fayyaz, A., Amin, SYM.: Ceramics

International, vol. 39, 2013, no. 4
[8] Fayyaz, A., Muhamad, N., Sulong, AB., Rajabi, J., Wong, YN.: Journal of Materials Processing Technology, vol. 214, 2014, no. 7, p. 1436
[9] Merz, L., Rath, S., Piotter, V., Ruprecht, R., Ritzhaupt-Kleissl, J., Hausselt, J.: Microsystem Technologies, vol. 8, 2002, no. 2, p. 129
[10] Fayyaz, A., Muhamad, N., Sulong, AB., Heng, SY., Amin, SYM., Rajabi, J.: Ceramics International A, *v*ol. 41, 2015, no. 3, p. 3605
[11] Machaka, R., Ndlangamandla, P., Seerane, M.: Powder Technology, vol. 326, 2018, p. 37
[12] Mannschatz, A., Müller, A., Moritz, T.: Journal of the European Ceramic Society, vol. 31, 2011, no. 14, p. 2551
[13] Rota, A., Duong, TV., Hartwig, T.: Microsystem Technologies, vol. 8, 2002, no. 4, p. 323
[14] Liu, L., Loh, NH., Tay, BY., Tor, SB., Murakoshi, Y., Maeda, R.: Materials Characterization, vol. 54, 2005, no. 3, p. 230
[15] German, RM., Bose, A.: Injection molding of metals and ceramics. Princeton, New Jersey: Metal Powder Industries Federation, 1997

Powder Metallurgy Progress, Vol.18 (2018), No.2, p.103-110
http://dx.doi.org/10.1515/pmp-2018-0011

MICROSTRUCTURE AND MECHANICAL PROPERTIES OF Fe/MgO MICRO-NANO COMPOSITE FOR ELECTROTECHNICAL APPLICATIONS

R. Bureš, M. Fáberová, P. Kurek

Abstract

The composite based on the microns iron size powder and MgO nano-powder was prepared using pressing followed by conventional and microwave sintering. Microstructure of the composite was investigated to evaluate the changes induced by different sintering technology. Young's modulus, flexural strength and hardness of composites were analyzed to investigate the mechanical properties in dependence on MgO content, as well as in dependence on the sintering method. Microstructure and mechanical properties as well as functional magnetic properties of prepared composites are discussed in the paper. The main benefit of microwave heating found within process time shortening was confirmed in the case of the microwave sintered Fe/MgO composite.

Keywords: soft magnetic composites, microwave sintering, microstructural analysis, mechanical properties, functional properties

INTRODUCTION

L.J. Huang in his work [1] asks the question: "Microstructurally inhomogeneous composites: Is a homogeneous reinforcement distribution optimal?". A wide range of uniquely multi-scale structures have been successfully designed and fabricated by tailoring reinforcement distribution for discontinuous metal matrix composites in order to obtain superior performance, focusing on mechanical behaviour of the materials. There are a lot of functional composites, where electrical, magnetic or other physical properties are essential for application. Controlled microstructural inhomogeneity can help to improve the desired properties of functional composites. One of the functional materials is soft magnetic composites (SMC). The concept of SMC is based on the ferromagnetic powder particle surrounded by dielectric thin film [2]. Consolidation of this powder creates a metal matrix composite with a dielectric network. The high resistivity of the SMC is a way to achieve lower Eddy current losses. The main goal is to make these materials suitable in AC applications of middle or higher frequencies.

The fabrication of an as thin as possible dielectric layer and its preservation during powder consolidation is a key problem of these materials. Soft magnetic powders with ceramic secondary constituent are powder materials characterized by limited compressibility [3-4]. Compaction of these powders leads to low green density. The result of the specific sintering process, where an iron-iron connection is unwanted, is relatively high porosity of the final SMCs. High porosity means low permeability and magnetic flux density. Mechanical properties of SMCs are low due to the brittle network as well as high rate of porosity.

Radovan Bureš, Mária Fáberová, Pavel Kurek: Institute of Materials Research, Slovak Academy of Sciences, Košice, Slovak Republic

Advanced powder metallurgy techniques can contribute to find solutions. One of the progressive sintering methods, which apart from process time shortening can help to preserve nano-structures in the sintering process, is microwave heating technology [5-6]. This work is focused on investigation of microstructure, electro-magnetic and mechanical properties of SMC based on pure iron micro-powder and high dielectric MgO nano-particles, prepared using traditional sintering as well as microwave sintering process.

EXPERIMENTAL MATERIALS AND METHODS

Technically pure Fe micro-particles (ASC 100.29, Höganäs AB, median size of powder particles $d_{0.5}$=100 μm) were dry coated by MgO nano-particles (MTI Corp., mean size d=30 nm, narrow distribution) using the Resonant Acoustic Mixing method in a Resodyn LabRAM mixer. Fe/MgO powders with 1, 2, 3, 5, 10 and 13.85 wt.% of MgO content were uniaxially cold pressed at a pressure of 600 MPa. Green compacts were sintered using a muffle furnace (conventional sintering further CS) at 600ºC, for 60 minutes, in a dry air atmosphere. Microwave sintering (further MWS) was provided in the multimode microwave cavity with controlled power from 300 W to 3 kW at a constant temperature of 600ºC for 15 minutes, in dry air atmosphere. The temperature in MW oven Hamilab V3000 was measured by IR pyrometer.

The hardness HV10 of cylinder samples with diameter size of 10 mm and height of 3 mm was tested by hardness tester LM 700AT. The elastic properties of prism bar sample size of 4x5x20 mm and ring samples` size of outer diameter 28 mm, inner diameter 25 mm and height of 3 mm were measured by non-destructive impulse excitation technique according ASTM E1876 using Buzz-o-Sonic equipment. Transverse rupture strength (TRS) was measured by 3 point bending test using universal testing machine LabTest 5.600 ZL. Light microscopy (LM Olympus GX71) and scanning electron microscopy (SEM JEOL JSM-7000F with EDS analyzer Inca) were used to investigate microstructure of the composite. Coercive force was measured by Coercive force meter DX-320 using a method of measurement of the coercivity of magnetic materials in an open magnetic circuit IEC 60404-7.

RESULTS AND DISCUSSION

Microstructure observation in Fig.1 and 2 show the network of secondary phase at the origin particle boundaries. Polarized light was used to study the distribution of secondary phase and porosity. Secondary phase was observed in the range of colours from light yellow to light grey in contrast to the dark brown iron matrix and black pores. Fe-MgO interphase of the sintered composites were investigated by SEM and line EDS methods. Low MgO content 1-2 wt.% is insufficient to avoid creation of iron-iron connections in both CS and MW sintering processes. Increased MgO content to 3 wt.% creates a continuous network of secondary phase. Increasing MgO content above 3 wt.% leads to the creation of thick interphase as well as to MgO cluster formation. Porosity depends on MgO content as well as on sintering technology. Pores are small and localised in three particle connection regions. In the case of CS composites, increasing MgO content increases porosity of the composites. Pores are larger in the composite with higher MgO content. Porosity was observed in interphase at higher MgO content in the composite. MW sintered composite is characterized by lower porosity in comparison to CS composite at the same MgO contents. A small addition of MgO content to 2 wt.% decreased the porosity of the composite. Interphase regions of MW composites are more compact with relatively more regular thickness in comparison to CS composites.

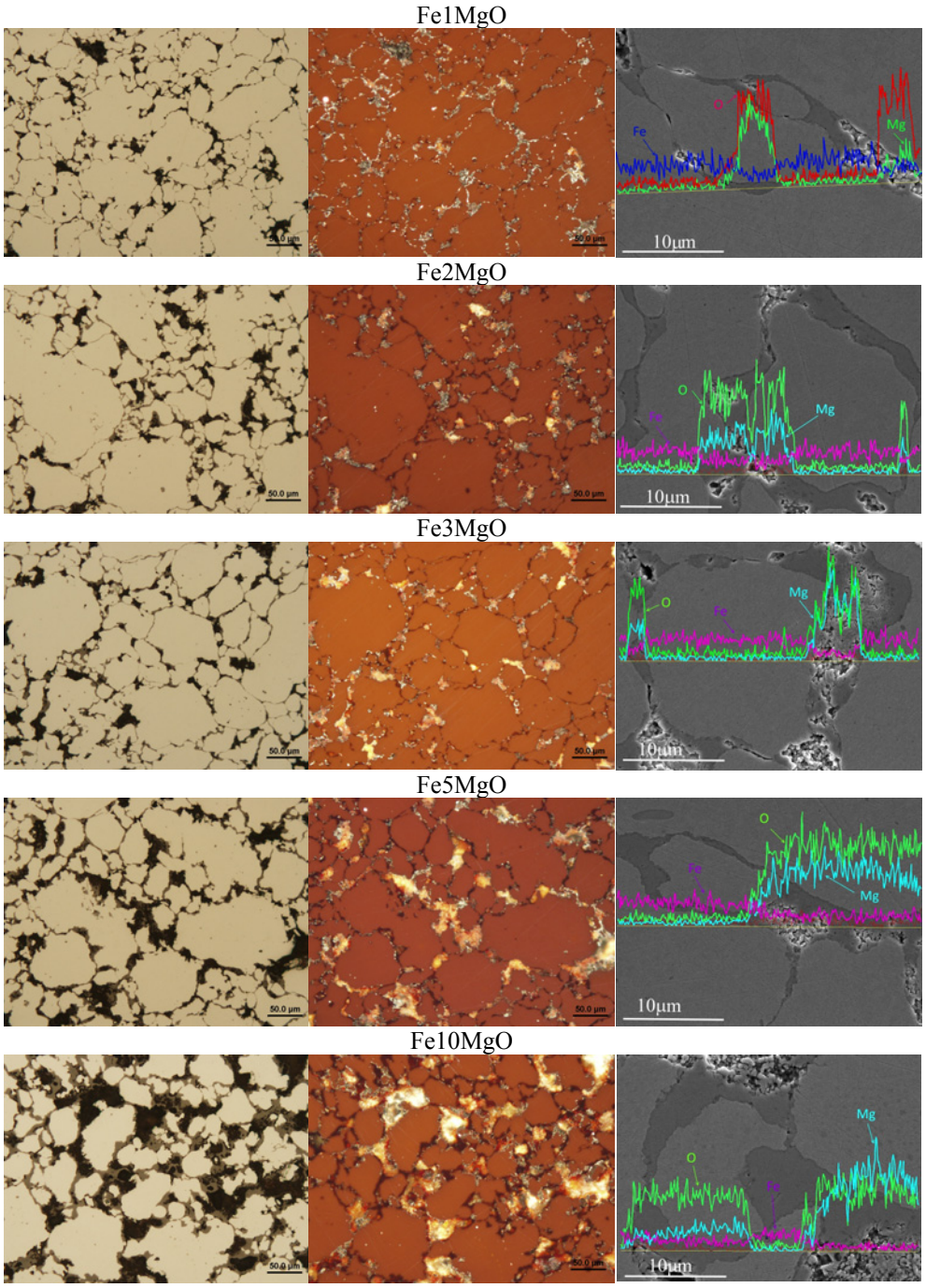

Fig.1. Microstructure and line EDS analysis of conventional sintered Fe/MgO composites.

Fe1MgO

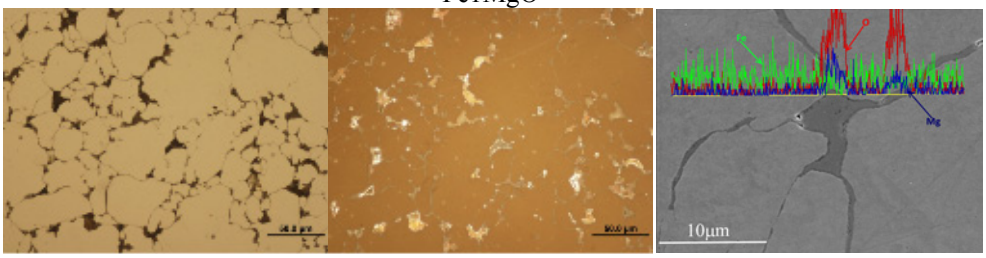

Fe2MgO

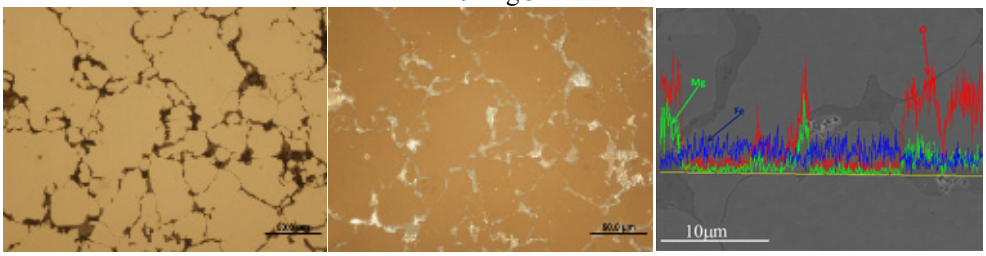

Fe3MgO

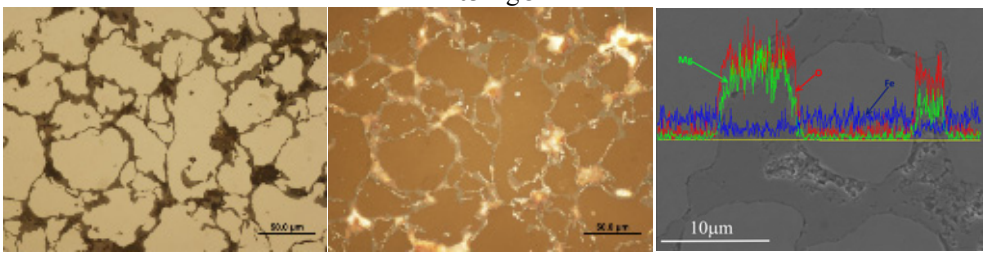

Fe5MgO

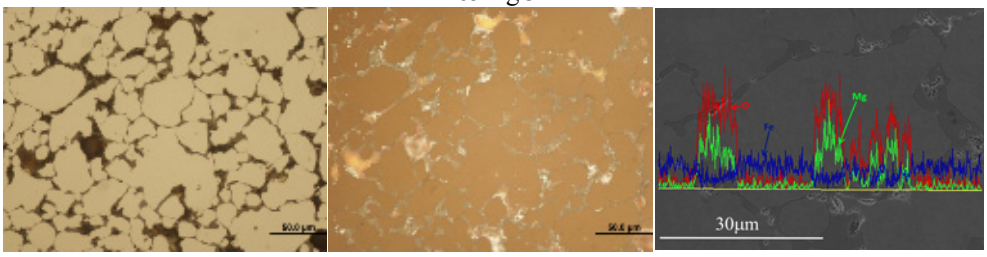

Fe10MgO

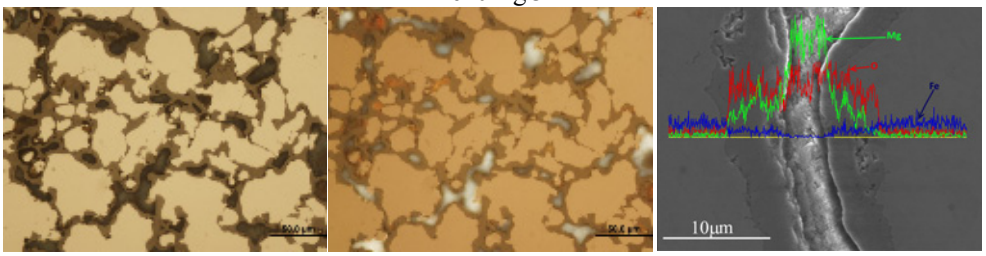

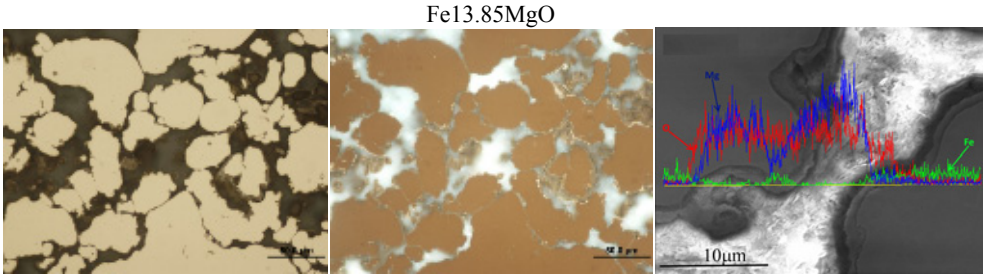

Fig.2. Microstructure and line EDS analysis of microwave sintered Fe/MgO composites.

Density values (in Fig.3.) confirm higher relative density of MWS composite in comparison with CS composite as well as in comparison with Fe/MgO green compacts. On the other hand, relative density values of the CS composites are lower than that of green compacts, because voids in the interphase decrease the density values especially at higher MgO content above 3 wt.%. The rise in value of Young's modulus after CS and MW sintering (in Fig.4.) confirms heat induced densification of MgO based ceramic phase in both sintering processes. Decreasing Young`s modulus in dependence on MgO content indicates increasing porosity values. Porosity has stronger influence on elastic properties than increasing content of MgO ceramic phase as it was calculated by Manoylov et al. [7].

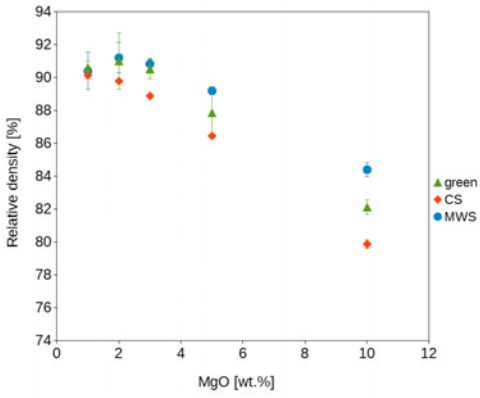

Fig.3. Relative density of the green compact, CS and MWS composites.

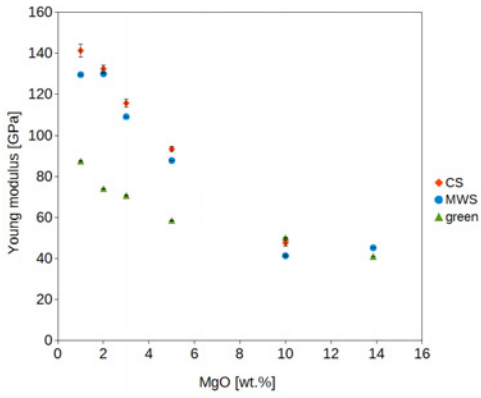

Fig.4. Young modulus of the green compact and sintered composites.

Analogous to Young`s modulus is the tendency of bending strength values in Fig.5. Strength represented by TRS value is related to the strength of secondary phase network. There are not Fe-Fe connections at higher MgO content, that is why TRS value decreases rapidly with an increased MgO content. Higher content of MgO means higher porosity, high porosity leads to lower elastic properties as well as lower mechanical strength. There is no significant difference in the TRS values of CS and MWS composites. More significant influence of sintering technology can be observed in the case of the hardness measurement. CS composite is characterized by two typical hardness values, which in Fig.6. represent Fe matrix (CS-1) and MgO based secondary phase (CS-2). Hardness values of the secondary phase of MWS composite (MWS-2) are considerably

higher. The MW sintering process together with higher MgO content induces formation of a microstructure region characterized by low hardness value (MWS-3), while hardness value of the Fe matrix remains the same in both sintering processes. Mechanical properties of the soft magnetic composites are relatively low in comparison with sintered metals or structural composites. Functional properties are crucial to the application of SMC. However, mechanical properties have to fulfill minimal requirements which depend on the concrete type of application in electrotechnics. Functional properties of the SMCs are based on the balance of electric resistivity, magnetic permeability, coercivity and magnetic flux density. DC resistivity and coercive force measurement were used to investigate a basic electromagnetic properties development in dependence on MgO content and sintering technology.

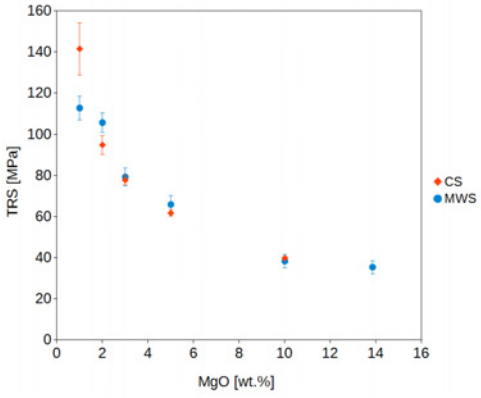

Fig.5. Transverse rupture strength of the sintered composites.

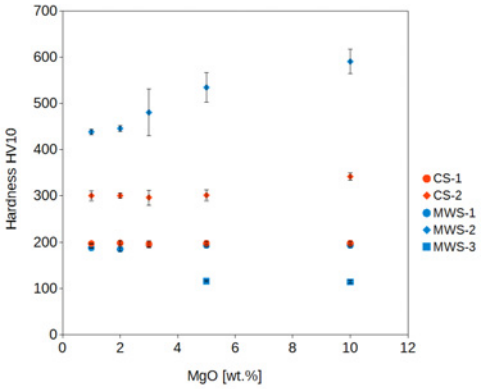

Fig.6. Hardness of the sintered composites.

Resistivity of the sintered composites is from 3 to 5 orders higher than that of green compacts as is shown in Fig.7. It was expected, because the result of the densification process during sintering is formation of Fe-Fe contacts to a certain extent. Resistivity of MWS composite Fe/3MgO is more then one order higher than that of Fe/2MgO, which confirms continuous dielectric network formation at MgO content above the value of 2 wt.%. In the case of conventional sintering it is necessary to use higher MgO content to create an effective dielectric network. Higher resistivity of CS composite at High MgO content (10 wt.%) is induced by higher porosity of CS in comparison to MWS composite. High resistivity created by high porosity is unwanted, because there can be expected a significant decrease of permeability in this case.

Coercivity as low as possible is required for soft magnetic composites. In Figure 8 it is shown that Fe/xMgO green compacts have coercivity force value circa 350 A/m. Coercivity of the green compact is influenced by cold pressing. Restoration and recrystallyzation processes during sintering are needed to decrease the coercivity value. Coercive forces decrease in CS composite in dependence on MgO content up to a value of 5 wt.%. In the case of MWS composite, coercive force decreases with increasing MgO content to a value of 3 wt.% MgO. Higher content of MgO above 3 wt.% or 5 wt.% leads to a rapid increase of coercive force of both CS and MWS composites. The most significant increase of coercivity can be observed in the case of MWS Fe/10MgO composite. Two factors can be responsible for the rise of coercive force values. The first factor is

uncompensated mechanical stress in the sintered composite as a result of a different temperature expansion coefficient of primary and secondary phase. The second factor is additional phase formation in the sintering process. This additional phase can be non-stochiometric $MgFe_2O_4$ spinnel ferrite as it is shown in the study of Deraz etal. [8]. The cubic spinnel phases of $MgFe_2O_4$ are formed by microwave heating at 500ºC for low soaking time of 10 min as it was confirmed in [9]. More intensive magnesium ferrite spinnel formation can develop higher residual thermal stresses in MWS composite, which result is higher coercive force.

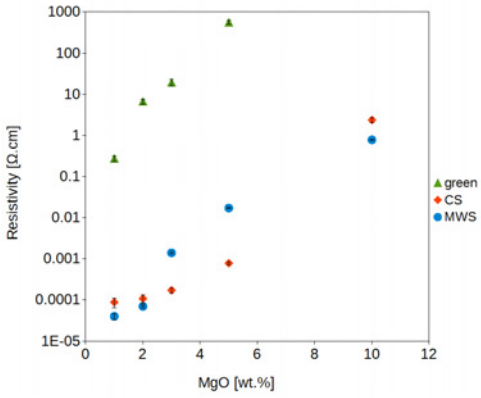

Fig.7. Resistivity of the green compact and sintered composites.

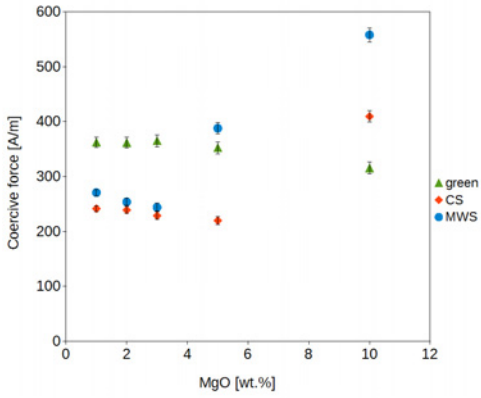

Fig.8. Coercive force of the green compact and sintered composites.

CONCLUSIONS

Soft magnetic micro-nano Fe/xMgO (x is from 1 to 13.85 wt.%) composite was prepared using cold pressing followed by traditional sintering as well as microwave sintering. Microstructure, mechanical and electro-magnetic properties were investigated to clear the processes of functional properties formation during sintering. Mechanical properties of Fe/MgO composite based on a lower content of MgO about 2 wt.% are comparable to current industrial soft magnetic composites. Higher contents of MgO above 3 wt.% MgO are typical of high resistivity and low coercive force values. The microwave sintering process helps to improve continuity of dielectric secondary phase network as well as contributes to a higher density of the composite, while process time is 5 times shorter in comparison to the conventional sintering process. An advantage of Fe/MgO soft magnetic composite is high temperature stability. Heat treatment at high temperature contributes to structure recovery, stress relief, thus give the possibility to optimize magnetic properties of the composite for specific applications.

Acknowledgements

This work was supported by the Scientific Grant Agency of the Ministry of Education, Science, Research and Sport of the Slovak Republic and the Slovak Academy of Sciences, project No. VEGA 2/0108/18 and the Slovak Research and Development Agency, project No. APVV-15-0115.

REFERENCES

[1] Huang, LJ., Ceng, L., Peng, HX.: Progress in Materials Science, vol. 71, 2015, p. 93
[2] Périgo, EA., Weidenfeller, B., Kollár, P., Füzer, J.: Applied Physics Reviews, vol. 5, 2018, 031301
[3] Sunday, KJ., Taheri, ML.: Journal of Magnetism and Magnetic Materials, vol. 463, 2018, p. 1
[4] Bureš, R., Fáberová, M. In: PM2010 World Congress – Compaction Equipment. Florence, 10.-14.10.2010. EPMA, 2010, CD
[5] Oghbaei, M., Mirzaee, O.: Journal of Alloys and Compounds, vol. 494, 2010, p. 175
[6] Bureš, R., Fáberová, M., Kollár, P., Füzer, J., Dobák, S., Onderko, F., Kurek, P.: Acta Physica Polonica A, vol. 131, 2017, p. 780
[7] Manoylov, AV., Borodich, FM., Evans, HP.: Proceedings of the Royal Society A, vol. 469, 2013, p. 1
[8] Deraz, NM., Abd-Elkader, OH.: International Journal of Electrochemical Science, vol. 8, 2013, p. 8632
[9] Chandra Babu Naidu, K., Madhuri, W.: Materials Today: Proceedings, vol. 3, 2016, p. 3810

Powder Metallurgy Progress, Vol.18 (2018), No.2, p.111-115
http://dx.doi.org/10.1515/pmp-2018-0012

PREDICTION OF WEAR BEHAVIOR IN POROUS SINTERED STEELS: ARTIFICIAL NEURAL NETWORK APPROACH

Hassan Abdoos, Ahmad Tayebi, Meysam Bayat

Abstract

Due to the increasing usage of powder metallurgy (PM), there is a demand to evaluate and improve the mechanical properties of PM parts. One of the most important mechanical properties is wear behavior, especially in parts that are in contact with each other. Therefore, the choice of materials and select manufacturing parameters are very important to achieve proper wear behavior. So, prediction of wear resistance is important in PM parts. In this paper, we try to investigate and predict the wear resistance (volume loss) of PM porous steels according to the affecting factors such as: density, force and sliding distance by artificial neural network (ANN). ANN training was done by a multilayer perceptron procedure. The comparison of the results estimated by the ANN with the experimental data shows their proper matching. This issue confirms the efficiency of using method for prediction of wear resistance in PM steel parts.

Keywords: Wear Behavior, Powder Metallurgy Steels, Artificial Neural Network.

INTRODUCTION

The economic factors, the production value, proper quality and gaining of market share are important issues that need to be addressed in order to manufacture parts in today's developing industry. Among the various methods, powder metallurgy (PM) is an efficient process for manufacturing the parts, given the aforementioned aspects. Powder metallurgy is a method for manufacturing metal and ceramic parts which is essentially based on the compaction of powder materials and sintering them below the melting temperature. Economic justification of the use of powder metallurgy is based on the production circulation. Therefore, the use of powder metallurgy is important in the production of automobile parts since this industry has a remarkable annual circulation of production [1, 2].

Powder metallurgy steels are widely used to operate under sliding, rolling or abrasive wear conditions such as gears and teeth. For this reason a deep understanding of their tribological behaviour is very important [3]. The wear of a solid surface is caused by contact with another surface. This process takes place by a mechanical contact between two surfaces. In powder metallurgy steels, porosity and microstructure are the most important factors which control the wear behaviour. Other factors that affect wear behaviour include: alloy elements, wear rate and coating [1]. The wear phenomenon has various mechanisms which include: abrasive, adhesive wear and surface fatigue.

Hassan Abdoos: Faculty of New Sciences and Technologies, Semnan University, Semnan, Iran.
Ahmad Tayebi, Meysam Bayat: Faculty of Material Engineering and Metallurgy, Semnan University, Semnan, Iran.

The phenomenon of a wear is one of the problems that the industry has been facing for a long time and it has been a major part of the destruction in the industry [4]. Given the expansion of the use of parts manufactured by PM method, it is of great importance to control the wear behaviour of these parts. On the other hand, performing experimental wear tests and manufacturing standard samples are two costly processes. According to these issues, using solutions that can predict the wear resistance of PM components without performing empirical tests and by using valid data in this area will be very promising.

Artificial neural networks (ANN) are new computing systems that recognize the algorithm through existing information processing. Then, the ANN can predict the output responses through complex systems. This system, inspired by biological neural networks, consists of a large number of processing elements called neurons. Using computer programming, one can design a data structure that works like neurons. In order to develop a training algorithm, one should create a network of interconnected neurons and train the network by applying this algorithm [5].

In this research, an artificial neural network is used to predict the wear behaviour of steels that produced by powder metallurgy process. For this purpose, multi-layered perceptron synthetic method has been used for network training. As mentioned earlier, density, force and slid distance are among the most important factors affecting the wear resistance of powder metallurgy parts; therefore, these factors are regarded as inputs, while the lost volume (estimated values) is regarded as artificial neural network output.

RESEARCH METHODOLOGY

In this paper, 60 data prepared for processing in the neural network were used. Data were collected by an empirical test performed using dry wear test on porous powder metallurgy steels [6]. It should be pointed out that the data use to involve low-alloy steel containing carbon, Cr and Mn.

In this paper, to predict the wear resistance of Fe-C-Cr-Mn steel the multilayered perceptron neural network, which contains 5 neurons in the hidden layer, have been used. Figure 1 shows the structure of the neural network with a single hidden layer. The bond strength between the two neurons is represented by weight (w_{ij}). The Equations (1) and (2) indicate the relationship between the input, the hidden layer and the output. The three-layered network demonstrated in Figure 1 has an input layer, an output layer and a hidden layer [7].

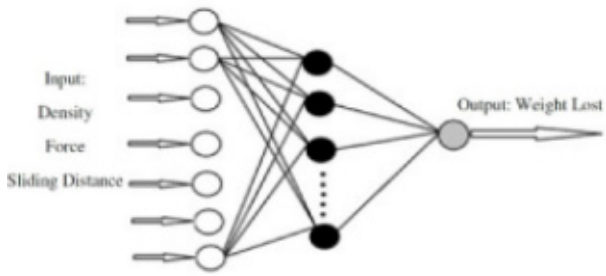

Fig 1. The structure of a perceptron neural network with a hidden layer [7].

$$a_1 = f_1(IW_{1.1} \times P + B_1) \quad (1)$$
$$a_2 = f_2(LW_{1.1} \times P + B_2) \quad (2)$$

The coding process was performed by MATLAB for artificial neural networks. Input and output data were normalized in order to better train the network in the interval [-1, 1], using the Equation (3) [5].

$$x_n = \frac{(x - Min\ x)}{(Max\ x - Min\ X) \times 2} - 1 x_n = \frac{(x - Min\ x)}{(Max\ x - Min\ X) \times 2} - 1 \quad (3)$$

In order to train the network and to test the accuracy of the program, 48 data (80% of the data) and 12 data (20% of the data) were used, respectively. The activation function in the network structure is known as Tangent Sigmoid function, shown in Equation (4) [8]. In order to minimize the output error of the neural network, the mean square error (MSE) is used which is shown in Equation (5).

$$tansig\ (n) = \frac{2}{(1 + exp(-2n))} - 1 tansig\ (n) = \frac{2}{(1 + exp(-2n))} - 1 \quad (4)$$

Where $n = w_{ij} \times u_i + b_i$.

$$MSE = \frac{1}{n} \sum_{j=1}^{n} (t_j - O_j)^2 MSE = \frac{1}{n} \sum_{j=1}^{n} (t_j - O_j)^2 \quad (5)$$

In the Equation (5), t, O and n represent the target value, output value, and the number of artificial neural networks outputs, respectively.

RESULT AND DISCUSSION

The results of artificial neural network training are as follows: The reason why the network is stopped is the number of iterations of the network (Epoch). The mean square error in the network training stage was 0.0078, while it was calculated to be 0.011 for the network test. The number of network training iterations, the network performance, the network derivative and the Mu is 1000, 0.00783, (at 0.000554 and 1×10^{-4}, respectively).

The Figure 2 shows the output normalization (Ytr) and the network training output (YtrNet), which are demonstrated by the red circle and the blue square, respectively. Figure 3 indicates the output normalization (Yts) and the network test output (YtsNet), which are represented again with red circles and blue squares. As shown in Figures 2 and 3, the output diagram and the training diagrams are relatively consistent which indicates the proper training and testing of the network up to this stage.

Figures 4 and 5 show the training and testing of the neural network, respectively. This includes the normalized value of the predicted fatigue limit based on the normalized value of the actual fatigue limit. The line plotted in Figures 4 and 5 shows the ideal state. The higher the density around the axis plotted, the better the prediction of the network.

The Figure 6 shows the mean squared error diagram based on the number of network training iterations. The diagram shows that the mean square error has the lowest value in 1000 iterations. The regression diagram is presented in the Figure 7. This diagram shows the deviation or regression from the ideal state, which is R = 1. This quantity corresponds to 0.97912. In the diagram, the closer the data diagram to the regression line, the better the training of the diagram. It ultimately indicates that the predicted values have a slight difference with the actual values obtained from the experimental test.

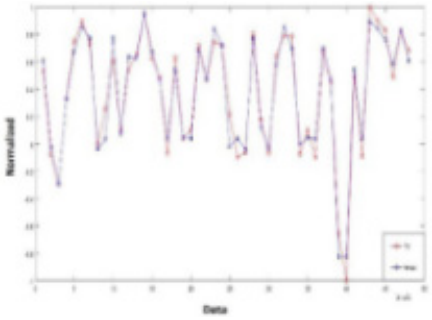

Fig.2. The output diagram and network training output.

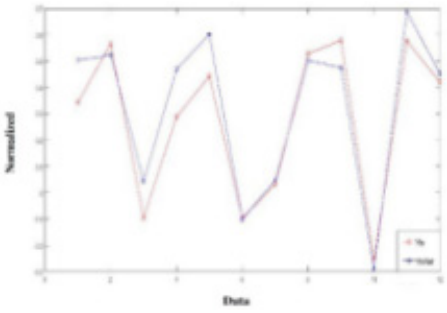

Fig.3. The output diagram and network test output.

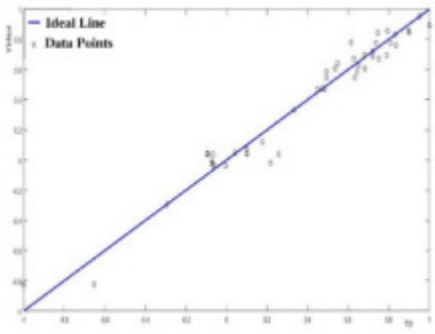

Fig.4. The normalized value of the predicted fatigue limit based on the normalized value of the actual fatigue limit in the network training process.

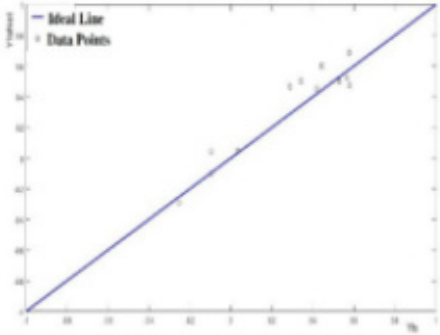

Fig.5. The normalized value of the predicted fatigue limit based on the normalized value of the actual fatigue limit in the network testing process.

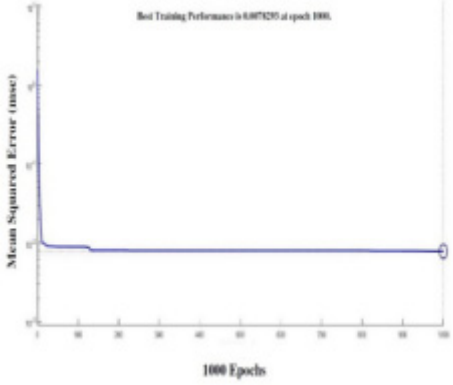

Fig.6. Mean square error diagram based on the number of network training iterations.

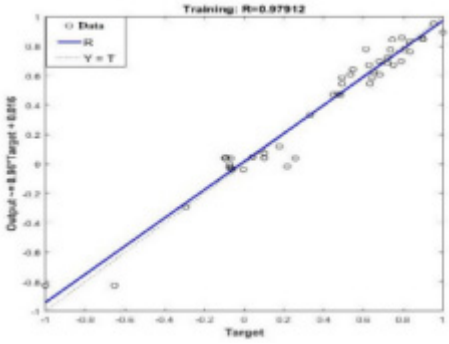

Fig.7. Regression diagram.

CONCLUSION

Wear resistance is one of the most important factors in the failure of industrial materials. The experimental tests are performed to measure this feature at a high cost. Therefore, artificial intelligence applications are used to predict the features of different parts. In this study, an artificial neural network was designed to estimate the rate of wear based on density, slide distance and force. The neural network was optimized with 5 neurons in the hidden layer. Furthermore, 48 data and 12 data were used in the training and the test processes, respectively. The accuracy of the network was measured during the test and training with the mean square error value. The Tangent Sigmoid function was used in the structure of this network (hidden layer cells). In order to facilitate the processing, data were normalized and then used in the hidden layer. According to the results, the used neural network is able to accurately estimate and predict the wear rate of the PM steels.

REFERENCES

[1] Khorsand, H., Abdoos, H.: The mechanical behavior and fatigue of porous sintered steel, K. N. Toosi university of Technology press, Tehran, Iran, 2015
[2] Khorsand, H., Abdoos, H., Amirjan, M.: Metallurgical Engineering Journal, vol. 43, 2011, p. 3
[3] Aliabadi, A., Heydarzadeh Sohi, M., Ghambari, M., Sheikhi Moghadam, K.: Advance Material, vol. 7, 2017, no. 28, p. 27
[4] Sahri, SM., Ghayour, H., Amini, K., Naseri, M., Morteza, H., Rastegari, H., Golparvar, M., Javaheri, V.: The effect of quench and temper treatment on microstructure characteristics and wear properties of a medium carbon- high chrome wear resistant steel, Steel symposium, Yazd, Iran, 2015
[5] Pourasiyayi, H., Pourasiyayi, H., Saghafiyan, H.: Advance Process in Material Science Quarterly, vol. 6, 2012, no. 2, p. 71
[6] Fallahdoost, H., Khorsand, H., Eslami-Farsani, R., Ganjeh, E.: Materials & Design, vol. 57, 2014, p. 60
[7] Asrardel, M.: Prediction of Combustion Dynamics in An Experimental Turbulent Swirl Stabilized Combustor with Secondary Fuel Injection. M.Sc. Thesis. Tehran : University of Tehran, 2015
[8] Matlab R2016a/ Help / tangsig

Powder Metallurgy Progress, Vol.18 (2018), No.2, p.116-120
http://dx.doi.org/10.1515/pmp-2018-0013

APPLICATION OF A LOW HEAT INPUT DEPOSITION PROCESS FOR REFURBISHMENT OF WORN PM FORMING DIES USING Fe-Ni BASED FILLER METAL

Mohamad Ebrahimnia , Hamzeh Baghjari, Mohamad Ajdari, Alireza Hajesmaeli, Milad Hojati

Abstract

Refurbishment of worn Dies is an interesting research area which also has high economic benefit. Material which is used in PM dies for compacting powders are high carbon steel which have very low weldabilitis. Due to the high hardness, high carbon content and martensitic microstructure, these Dies are very sensitive to the thermal shock produced from fusion welding. For successfully refurbishing the worn Dies, Fine spark deposition was used for deposition of a new layer on the cold work 1.2436 steel. Different heat inputs were used for deposition of nickel based material and finally microstructure and HAZ were studied. Results show the HAZ area is very narrow, free from cracks and HAZ microstructure is similar to the base metal. GTAW welding using same filler metal induced many cracks in HAZ of weld which is detrimental to the refurbished Die performance. Results show increasing heat input in Fine spark deposition can results in crack formation in HAZ even if the weld pool does not occurred in base metal. However these cracks are much smaller than those occurred in GTAW.

Keywords: Powder metallurgy, Fine spark deposition, Die, 1.2436 steel.

INTRODUCTION

AISI D6 or DIN 1.2436 is a 12% chromium alloy cold work tool steel which is used as die and punch in blanking, piercing and cold forming processes. This steel is widely used for powder shaping Dies manufacturing in powder metallurgy industry. Tool service life is limited by plastic deformations, wear and rupture due to the presence of high stresses and cracks. [1,2].

The as-cast microstructure is composed of ferrite, carbides especially Cr_7C_3, pearlite, and bainite with a hardness of 240 HV. Hardness after annealing at 800-840°C and slow furnace cooling will be approximately 225 brinell. Annealed microstructure consists of large amount of Cr_7C_3 carbides in an austenitic matrix. Hardening of this steel results in high hardness. Microstructure of double tempered sample consists of tempered martensite and fine distribution of chromium carbide particles [3].

Mohamad Ebrahimnia: Material engineering department, Tehran Science and research branch, Islamic Azad University, Tehran, Iran
Hamzeh Baghjari: Material Engineering, Tarbiat Modares University, Tehran, Iran.
Mohamad Ajdari: Material engineering department, Tehran Science and research branch, Islamic Azad University, Tehran, Iran
Alireza Hajesmaeli, Milad Hojati: Mashhad Powder metallurgy Company, R&D and Engineering department, Mashhad, Iran

Because of high hardenability and large amount of carbide particles, this tool steel has very low weldability. The weldability of steels with more than 0.2% carbon is usually considered to be poor. Hence, tool steels with 0.3–2.5% carbon are difficult to weld and many steel suppliers will actually recommend against welding. Depend on different situations, welding with arc welding processes required high preheating temperature near 200-250 C and sophisticated post weld heat treatment, which makes welding process very difficult [4].

One of the major drawback of arc welding processes e.g. GTAW is high volume of heat input and formation of weld pool which induces high heat affected zone area (HAZ). These areas are prone to severe cracking after welding if proper preheat and post weld heat treatment cannot be carried out.

Previous studies on welding precipitated nickel based super alloy using low heat input processes e.g laser welding and fine spark deposition showed promising results on crack free welding of these alloys. Beside low heat input fusion welding processes like pulsed laser welding, Fine spark deposition (FSD) is another low heat input process which makes it ideal as a coating and build up technology in many applications. Fine spark deposition has many applications in rebuilding and coating conductive materials. Because of its very low heat input, it is ideal for rebuilding metals which are susceptible to HAZ cracking [5,6].

In this process, very small droplets of molten metal are detached from rotating electrode, then transfer to the substrate and impact the substrate. This phenomenon induces such inherent defects like lack of fusion (LOF) and porosity in deposition. The researchers have not achieved great success for complete elimination of such defects in FSD overlay.

In a recent study by the author it was shown that IN738LC can be built up by Fine spark deposition (FSD) process and then subjected to pulsed laser fusion processing to improve the integrity of the FSD deposited layer [6]. It is found that the FSD material has more resistance to liquation and solidification cracking than the cast base metal. In the present study, FSD was used as a buildup technique for deposition high Ni-Cr steel based alloy on the 1.2436 tool steel for refurbishment of steel Dies used in powder metal pressing.

EXPERIMENTAL MATERIALS AND METHODS

The material used for this research was quench and tempered 1.2436 tool steel with chemical composition has shown in table 1. The filler metal which is used in fine spark deposition was a round cylindrical rod with 4 mm diameter with chemical composition shown in Table 1.

Tab.1. Chemical Composition Wt%.

Composition	C	Mn	Si	Cr	W	Ni
1.2436	2	0.2	0.2	11.5	0.7	-
FSD filler	0.11	1.67	0.68	15.2	-	35
GTAW filler	0.2	0.6	0.2	2	-	-

Heat treatment of steel was done in following manner:

- Annealing in 970 C
- Hardening 940 C, Quenching in oil
- Tempering in 450 C for 2 hours

Fine spark deposition was performed on a 2 mm diameter quench and tempered cast billets. FSD deposition was performed using a hand held gun with a co-axis shield gas

facility. Initially a number of tests were performed to establish a suitable FSD process window with respect to the appearance of the deposit for example surface roughness and spatter. For the experiments that are reported here, electrode rotation speed was 2500 rpm and electrical parameters were voltage of 40 volt, frequency of 110 Hz and duty cycle of 40 %. During FSD process argon shielding gas was fed to the surface with a flow rate of 15 liters/min.

For comparison of results, Micro GTAW using P20 filler wire was carried out with current if 30 A and pulsed frequency of 5 Hz. Composition of GTAW filler wire can be seen in Table 1.

A number of samples were taken for metallographic characterization of the as deposited fine spark buildup layer of steel. Some samples are studied for micro hardness test. Vickers micro hardness test was done using 200 g load and 15 s dwell time.

RESULTS AND DISCUSSION

The Figure 1 shows the microstructure of GTAW weld on high chromium steel. Microstructure of base metal consists of large amount of fine white chromium carbide particles embedded in tempered martensitic matrix.

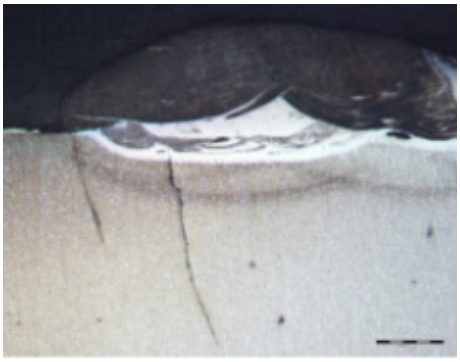

Fig.1. cracks in HAZ of 1.2436 steel weldment in GTAW process.

As it is clear, 2 large cracks are initiated from HAZ and propagate to the weld zone and base metal. These cracks show the welding impossible without preheat and post weld heat treatment.

The Figure 2 shows different areas in GTAW weldments in higher magnification. The thickness of HAZ beneath weld is about 200 µm. There is not considerable different between HAZ microstructure and base metal. This is because of very fast cooling rate in micro GTAW and low heat input in this process in comparison with GTAW process.

The Figure 3 shows the FSD microstructure and base metal. Form micrograph one can see there is not HAZ indication in the weldment and interface of rebuilding area has metallurgical bonding to the base metal. Although some crack like indication in upper part of coating can be detected, the entire coating has good fusion to the base metal.

There is no crack in base metal of FSD process and makes it ideal for rebuilding the worn areas of steel dies. Higher magnification of coating can be seen in Fig.4.

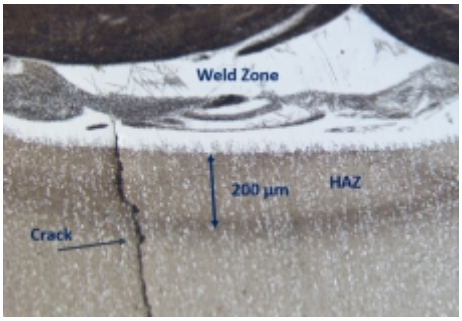

Fig.2. Different areas in GTAW weldments.

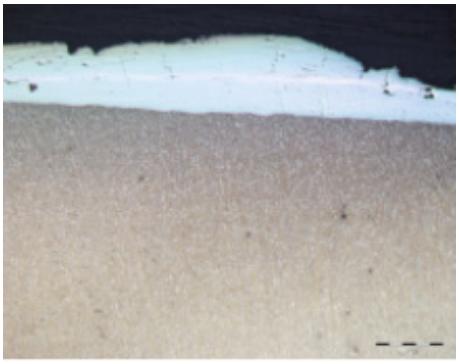

Fig.3. The FSD coating on the steel 1.2436.

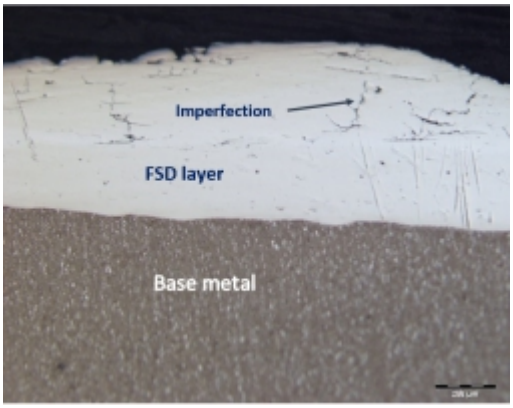

Fig.4. FSD layer which has some imperfection.

The FSD layer has some imperfection which are like cracks. However, these imperfection were detected also in previous studies [4,5].

Micro hardness results are shown in Table 2. In the GTAW sample, high hardness in HAZ and base metal along high tensile stress which is exerted on HAZ by shrinkage of weld metal during solidification can cause severe cracking in HAZ.

Tab.2. Microhardness results.

Avg. Hardness	Hardness 3	Hardness 2	Hardness 1	Hardness HVN
298	347	299	248	FSD layer
407	465	396	362	GTAW

Average hardness of base metal is about 550 HVN. HAZ hardness in GTAW has highest hardness e.g. 644 HVN. Because the weld metal has lower hardness than HAZ and base metal the crack blinded in weld metal. The crack formation is very feasible in High hardness HAZ and then it cannot resist cracking due to the high hardness and brittle microstructure.

Although hardness of FSD layer is lower than GTAW weld, hardness of FSD layer is acceptable. However, the hardness is much lower than base metal. The low heat input in FSD process makes the welding feasible without preheating the sample. Because the

deposition forms by depositing large numbers of tiny droplets of filler metal, the heat input per every single droplet is very small.

Figures 5 and 6 show an area of worn Punch dies and subsequent repair area by FSD process. Service work shows sound performance of repaired area under actual service condition.

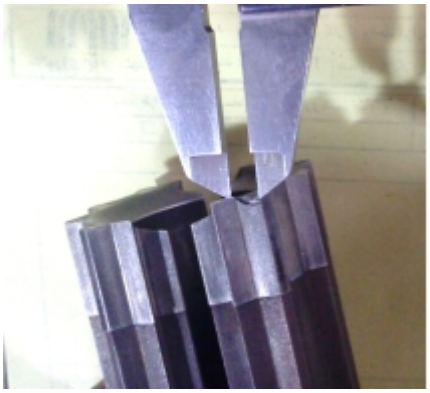

Fig.5. Worn area on the edge of steel 1.2436 die.

Fig.6. Repaired area before machining.

CONCLUSION

Weld deposition of steel 1.2436 using two different method show the effect of heat input on sound, crack free buildup of worn area. This work can be concluded as follows:

- The FSD process is used for deposition of high nickel chromium filler metal on 1.2436 steel without HAZ cracking.
- Micro GTAW process using steel filler wire results in HAZ cracking. High hardness of base metal and high amount of weld shrinkage can be the problem of arc welding of this alloy without preheat and post weld heat treatment.
- Service performance of refurbishment area shows acceptable weld overlay by FSD process.
- Low heat input, low tensile stress and very narrow HAZ have synergetic effect on crack free repair welding of high chromium steel using FSD welding without preheat and post weld heat treatment.

REFERENCES

[1] Thompson, S.: Handbook of mold, tool and die repair welding. Abington Publishing, Woodhead Publishing Ltd., 1999
[2] D6 tool steel. https://www.westyorkssteel.com/files/d6.pdf
[3] Goia, FA., Fernandes de Lima, MS.: Journal of ASTM International, vol. 8, no. 2, p. 1
[4] Ebrahimnia, M., Ghaini, FM., Shahverdi, HR.: Science and Technology of Welding and Joining, vol. 19, 2014, p. 25
[5] Ebrahimnia, M., MalekGhaini, F., Xie, YJ., Shahverdi, H.: Surface and Coatings Technology, vol. 258, 2014, p. 515
[6] Ebrahimnia, M., MalekGhaini, F., Xie, YJ., Shahverdi, H.: Science and Technology of Welding and Joining, vol. 21, 2016, no. 7, p. 570

Powder Metallurgy Progress, Vol.18 (2018), No.2, p.121-127
http://dx.doi.org/10.1515/pmp-2018-0014

NEW CHANCES FOR THE MASTERALLOY APPROACH

Raquel de Oro Calderon, Maryam Jaliliziyaeian, John Dunkley, Christian Gierl-Mayer, Herbert Danninger

Abstract

The Masteralloy (MA) alloying route has a great potential for reducing the alloying costs in sintered steels, while allowing the introduction of innovative alloying systems. However, in order to achieve an efficient use of the alloying elements, the particle sizes needed are often below 25 µm, which means that for standard gas atomization a significant fraction of the batch has to be discarded or at least recycled. This work evaluates the performance of steels containing MA powders obtained with a novel atomization technique (Ultra-High-Pressure Water atomization) that allows the production of low-cost powders with low oxygen contents, rounded morphologies and mean particle sizes as low as 6 microns. Mechanical properties, dimensional variations and interstitial contents were measured in steels containing different MA compositions sintered at either 1120 °C or1250 ºC in N_2-5H_2 atmospheres. Already with less than 3 wt.% of alloying elements these steels present excellent combinations of properties, reaching strength levels of 560-915 MPa and hardness 220-260 HV10, combined with elongations of 1.3-3.2% and impact energies around 20-30 J/cm2.

Kewords: Lean low alloy steels, Alloying design, Masteralloys, Mechanical properties

INTRODUCTION

The Masteralloy (MA) route applied to sintered steels consists on mixing Fe base powder with an MA powder that contains all alloying elements in a combined form. It allows the introduction of oxygen sensitive elements such as Si, Mn and Cr [1-3], which can significantly improve the properties of low alloy steels. The composition of the MA can be designed to promote the formation of a transient liquid phase that enhances sintering [4-11]. Other advantages of the MA route are the flexibility in the selection of the final composition and the possibility to retain the compressibility of the Fe base powder. The development of master alloys for PM steels has been a topic of research since the early 70's. At that time, some very interesting master alloys named MCM (Mn-Cr-Mo), MVM (Mn-V-Mo) and MM (Mn-Mo) were thoroughly studied for almost two decades, with the aim of using them in the production of highly loaded PM parts [1-3], but were eventually abandoned in the 90's due to the excessive tool wear caused by the very hard and angular MA powder particles (at that time produced by casting and then milling the ingots).

In the last two decades the use of gas atomization techniques has boosted the research in MA´s because it allows obtaining powder particles with adequate morphology and low oxygen contents.

Raquel de Oro Calderon, Maryam Jaliliziyaeian, Christian Gierl-Mayer, Herbert Danninger: Institute of Chemical Technologies and Analytics, Technische Universität Wien
John Dunkley: Atomizing Systems Limited, Sheffield, England
Presented at "PM Auto 2018", April 16-18, 2018, Isfahan, Iran

However, the process often yields particle size distributions centred at ~50-100 µm while for many applications the particle size needed to ensure a proper distribution of alloying elements during sintering is below ~25 µm. Therefore a significant fraction of the gas atomized batch has to be discarded or at least recycled.

This work reports the properties of steels containing MA powders produced using a newly developed atomization technique "Ultra High Pressure Water Atomization (UHPWA)".that allows obtaining MA powders with rounded morphologies, low oxygen contents (~1 %), small particle sizes and at relatively low production costs.

MATERIALS AND METHODS

The materials used in this study were produced from mixes containing Fe-0,5%C-4%MA pressed at 600 MPa in a double action press using die wall lubrication. Water atomized iron (grade ASC 100.29, Höganäs AB Sweden - O < 0.1wt.; %, C < 0.01wt. %) was used as base powder, and carbon was introduced as natural graphite (grade UF4, Kropfmühl). The characteristics of the master alloy powders used are presented in Table 1. Melting ranges of the master alloys were obtained through Differential Thermal Analysis (DTA) studies in Ar, carried out with a high-performance modular Simultaneous Thermal Analyzer Netzsch STA 449 C.

The MA powders were produced by Ultra High Pressure Water Atomization (UHPWA). This utilizes water pressures of 60-200 MPa and operates with induction melted batches of molten alloy, atomization being followed by dewatering and vacuum drying. As can be observed in Table 1, the oxygen values obtained are fairly low, and the MA powder particles present rather small particle size distributions and rounded morphologies (Fig. 1).

Tab.1 Characteristics of the master alloy powders used in this study.

Name	Nominal Composition	d10	d50	d90	O (%)	C (%)	Melting range
H45	Fe-32Cr-8Si-4C	3.21	7.84	18.4	0.14	4.01	1150-1220 ºC
H46	Fe-42Mn-6Si-0.4C	2.33	6.7	16.1	1.60	0.54	1120-1200 ºC
H47	Fe-28Mn-27Cr-6Si-3.7C	2.92	8.09	22.6	0.20	3.61	1095-1310 ºC

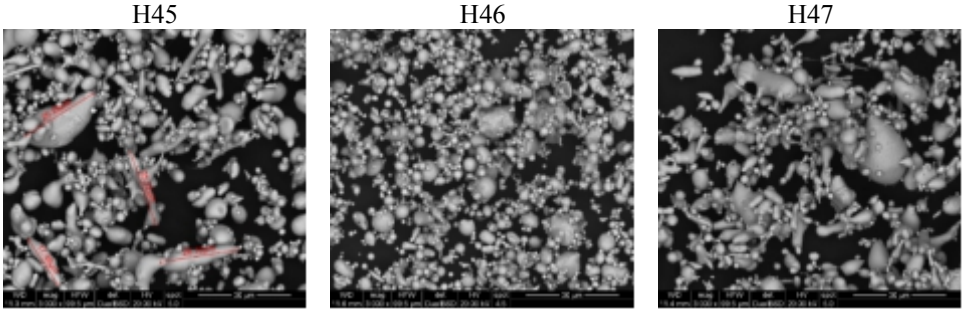

Fig.1. SEM images of the masteralloy powder particles.

Standard tensile test (ISO 2740) and impact test bars (ISO 5754) were produced for this study. Sintering was carried out in a lab scale furnace AHT Silitstabofen with gas-tight superalloy retort, at 1120 °C and 1250 °C under N_2-5H_2 atmosphere. The gas flow was introduced from the furnace outlet, and the samples were progressively pushed to the maximum temperature zone where they were kept for 30 min. The heating rate obtained using this procedure is estimated at around 30 K/min (~0.5 °/s). After the holding period at

temperature, the samples were cooled in a water-jacketed exit zone under the same protective atmosphere used for sintering. The linearized cooling rate obtained using this procedure is about 45 K/min (~0.75 K/s).

RESULTS AND DISCUSSION

Microstructures

The Figure 2 shows the microstructures of steels containing masteralloys sintered at 1120°C and 1250°C.

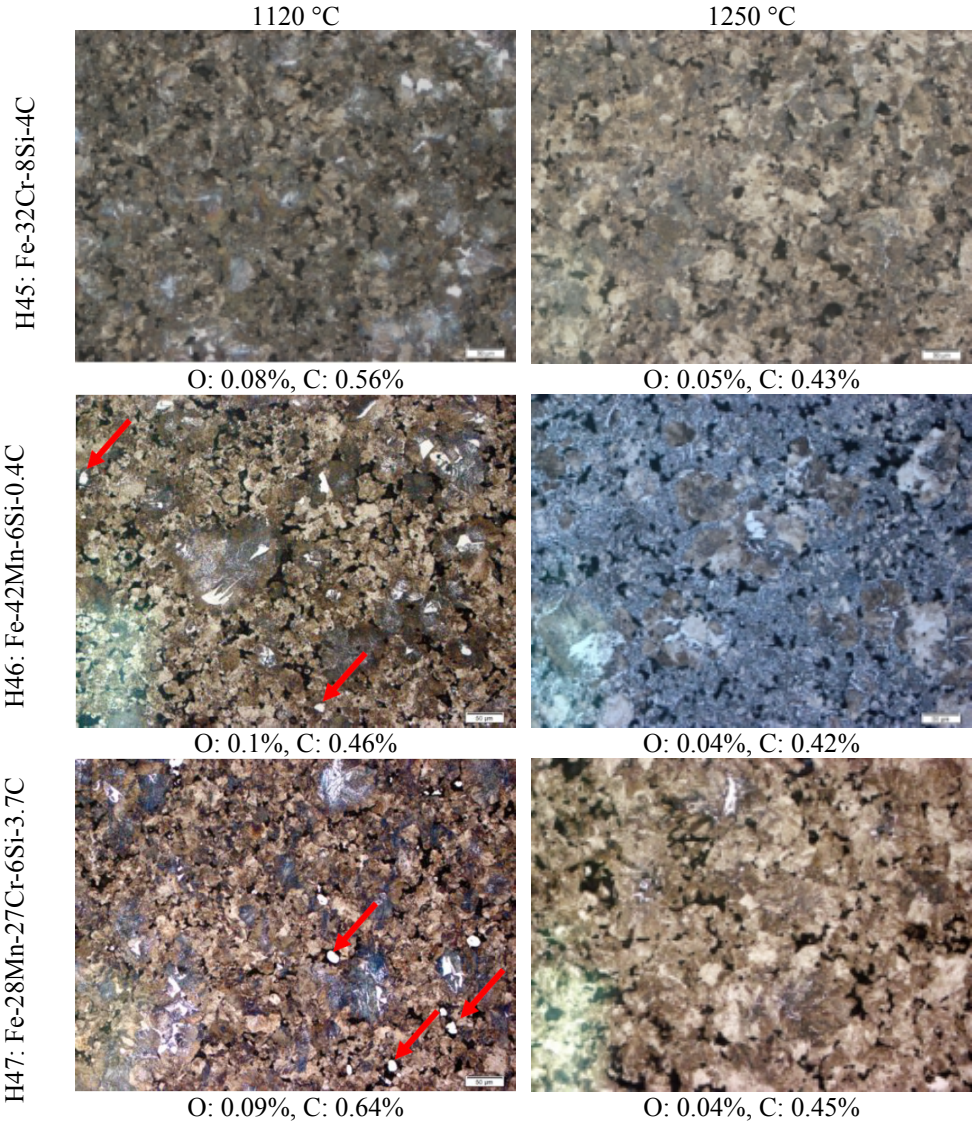

Fig.2. Microstructures and interstitial contents in steels containing masteralloys (Fe-0.5C-4MA) sintered at 1120 °C and 1250 °C for 30 min in N_2-5H_2.

The typical microstructure consists of fine perlitic phases in the cores of the Fe base powder particles, surrounded by areas with a higher amount of alloying elements in which harder microstructures are developed . The homogeneous distribution of these phases within the sample suggests a fairly good distribution of the alloying particles in the mix. At high sintering temperatures the porosity is more rounded, and the diffusion of alloying elements is improved, which is evidenced by the decrease in the amount of ferritic/perlitic areas. Undissolved masteralloy particles are clearly discernible in steels containing masteralloys H46 and H47 sintered at 1120 ° C, some of them have been marked with arrows in Fig. 2. This suggests that the sintering temperature/time has been insufficient to efficiently distribute the alloying elements present in the masteralloy.

Dimensional Changes and Density

Density and dimensional changes are represented in Fig. 3. In general, steels containing Fe-based masteralloys can give rise to swelling or shrinkage phenomena, depending on whether the swelling effect produced during the diffusion of alloying elements - or the melting of the masteralloy particles – can be or cannot be compensated by the shrinkage that takes place in the isothermal region. As the sintering phenomena are more activated at high temperatures, higher shrinkage effects (or lower swelling) are observed when increasing the sintering temperature. Dimensional changes -measured on the length of impact test bars - in steels containing H45 and H46 are around 0,1% or below. With these two masteralloys swelling is observed when sintering at 1120°C, while shrinkage takes place when sintering at 1250°C. Consequently, density increases with the sintering temperature, because the sintering phenomena are activated by the higher temperatures. The densities of steels containing H45 and H46 are in the range of 7.02-7.07 g/cm^3.

Swelling is observed in samples containing masteralloy H47 both at 1120 and - to a lower extent- at 1250°C. As a consequence, the sintered density is lower than the green density, and the densities achieved are below 7 g/cm^3.

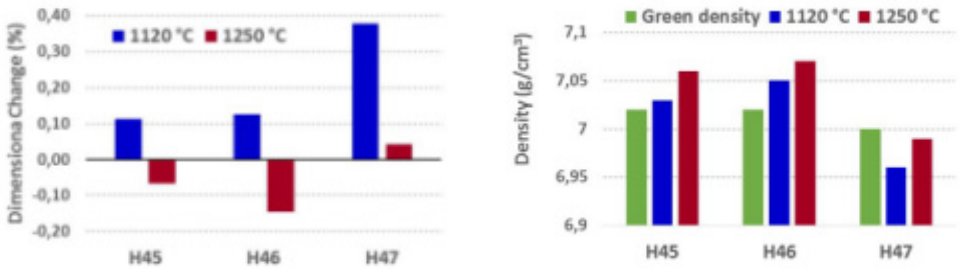

a) b)

Fig.3. Dimensional changes (a) and density (b) in steels containing masteralloys (Fe-0.5C-4MA) sintered at 1120 °C and 1250 °C for 30 min in N_2-5H_2.

Mechanical Properties

Mechanical properties (represented in Fig.4) are strongly influenced by the sintering temperature. On one hand this is because of the enhanced distribution of alloying elements at higher sintering temperatures, and on the other hand due to the higher densities and more rounded porosity.

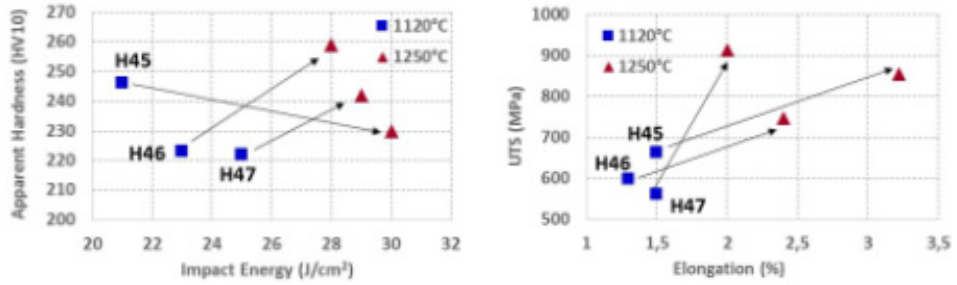

(a) (b)

Fig.4. Apparent Hardness vs. Impact Energy (a), and Ultimate Tensile Strength (UTS) vs. Elongation (b) in steels containing masteralloys (Fe-0.5C-4MA) sintered at 1120 °C and 1250 °C for 30 min in N_2-5H_2.

The as-sintered hardness values obtained (see Fig. 4a) are in the range of 220-260 HV10 which is in good agreement with the microstructures observed for these steels (see Fig.2). With masteralloy H45 the hardness decreases when increasing the sintering temperature. Apart from the decrease in the carbon content at 1250°C (due to the enhanced reduction of oxides at high temperatures) also the differences in the distribution of alloying elements play a role on this effect. At higher sintering temperatures, the alloying elements are more homogeneously distributed in the sample, and therefore the amount of highly alloyed (solution hardened) areas decreases, and so does the apparent hardness. Also local sinter hardening might play a role.

A different effect is observed in steels containing H46 and H47, for which the increase in the sintering temperature causes an increase in the hardness values. In this cases, as suggested by the microstructures from Fig.2, some masteralloy particles are still not dissolved in the Fe base powder, and therefore the alloying elements are not fully utilized. An increase in the sintering temperature promotes the homogenization of the alloying elements, resulting in a significant increase in the apparent hardness values. The highest hardness is observed in steels containing H46, in which bainitic microstructures are developed in the highly alloyed areas (see Fig.2).

The impact energy values obtained are reasonably high - 20-26 J/cm^2- already at 1120 °C (see Fig.4a). The higher sintered densities, more rounded porosity and lower carbon contents obtained when sintering at 1250 °C contribute to increased impact energy, that reaches values around 28-30 J/cm^2.

The Ultimate Tensile Strength (UTS) of steels sintered at 1120°C is around 550-700 MPa and is combined with elongations around 1.5%. By increasing the sintering temperature both the UTS and elongation values are increased, reaching UTS of 747-913 MPa combined with elongations above 2 %.

Comparison with commercial sintered steels

The Figure 5 shows a depiction of properties in which the steels produced in this study are compared with steels produced using commercial powders (data obtained from [12, 13]). As can be observed in Fig.5a, steels obtained using UHPWA-masteralloys (from this study) present very competitive UTS values with a very low content (below 3 wt.%) of inexpensive alloying elements (Cr, Mn, Si). In the graph from Fig.5a, the positioning of steels containing UHPWA masteralloys is similar to those obtained with Cr-prealloyed

powders with a similar amount of alloying elements (both for 1120°C and 1250°C sintering temperature).

A similar comparison is presented in Figs.5b and c, but in these latter cases UTS is represented against elongation (Fig.5b) and apparent hardness is plotted against impact energy (Fig.5c).

Excellent combinations of properties are observed in steels containing UHPWA master alloys, even when sintering at 1120°C, very competitive with those obtained with commercial powders and again comparable with Cr-prealloyed grades. At high sintering temperature (1250°C) the properties of steels containing masteralloys are boosted, presenting very interesting combinations of strength and ductility.

The fact that some of the masteralloy particles (H46 and H47) did not dissolve completely in the steel at 1120°C leaves some room for improvement. Working on the design of the masteralloy composition, it might be possible to obtain a better distribution of alloying elements at low sintering temperatures, thus positioning even better on the property map the steels obtained following the masteralloy route.

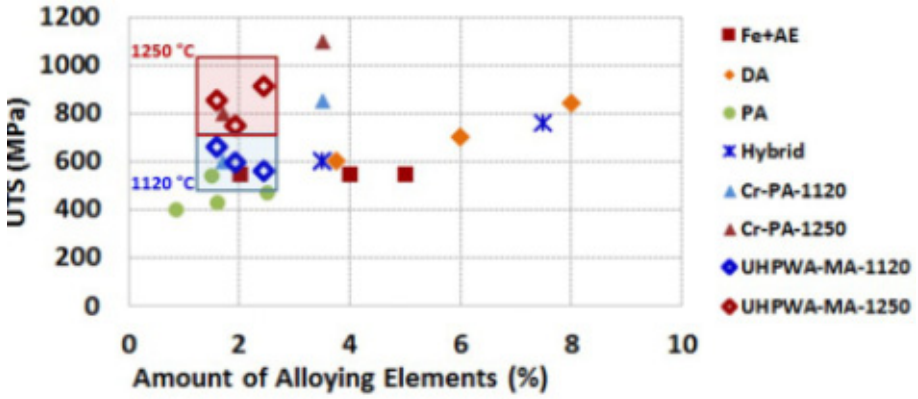

(a) UTS vs % Alloying Elements

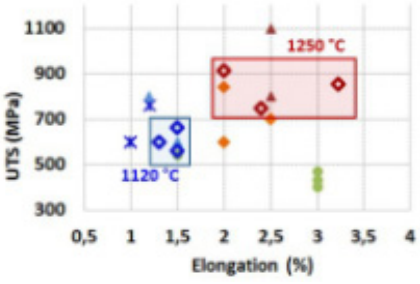

(b) UTS vs Elongation (%)

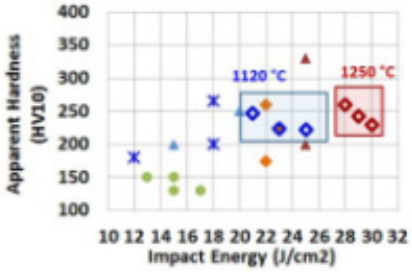

(c) Apparent Hardness vs Impact Energy

Fig.5. Comparison of properties of the steels obtained in this study with steels produced under similar conditions using commercial powder grades.

*Fe+AE: Fe with alloying elements Mo, Ni, Cu, DA: diffusion alloyed, PA: conventional prealloyed grades, Cr-PA Cr prealloyed powders sintered either at 1120 °C or at 1250 °C, UHPWA-MA: steels from this study sintered either at 1120 °C or at 1250 °C.

CONCLUSION

A newly developed atomizing technique named Ultra High Pressure Water Atomization (UHPWA), which allows economic production of masteralloy powders with mean particle sizes as low as 6 μm, has been applied to produce the masteralloy powders used in this study. After sintering at 1120°C and 1250ºC for 30 min in N_2-5H_2, the sintered steels prepared using these masteralloys show excellent combinations of properties: UTS~ 560-915 MPa, hardness ~220-260 HV10, elongation ~1.3-3.2% and impact energy ~20-30 (J/cm2). With less than 3 wt.% of inexpensive alloying elements these steels present combinations of properties that reach or even surpass the properties of steels obtained with commercial powders. In some of the steels produced, the masteralloy particles were not completely dissolved when sintering at 1120°C, which indicates that a re-design of the alloying composition to promote the diffusion of alloying elements at lower temperatures (by e.g. the formation of a liquid phase) could result in an even better combination of properties for low temperature sintering cycles.

Acknowledgement

The authors want to acknowledge financial support from the European Union through a Marie Sklodowska-Curie scholarship (Grant agreement PIEF-GA-2013-625556) awarded to one of the authors (Raquel de Oro Calderon)

REFERENCES

[1] Zapf, G., Dalal, K.: Modern developments in powder metallurgy, 1977, p. 129
[2] Schlieper, G., Thümmler, F.: Powder Metallurgy International, vol. 11, 1979, p. 172
[3] Banerjee, S., et al.: Progress in Powder Metallurgy, vol. 13, 1980, p. 143
[4] Fischmeister, HF., Larsson, LE.: Powder Metallurgy, vol. 17, 1974, p. 227
[5] Mocarski, S., et al.: Powder Metallurgy, vol. 39, 1996, p. 130
[6] Klein, AN., Oberacker, R., Thummler, F.: Modern Developments in Powder Metallurgy, vol. 16, 1985, p. 141
[7] Danninger, H.: Powder Metall. Int., vol. 20, 1988, no. 1, p. 21
[8] Tojal, C., Gomez-Acebo, T., Castro, F.: Progress in Powder Metallurgy, Pts 1 and 2, vol. 534-536, 2007, p. 661
[9] Castro, F., et al.: Progress in Powder Metallurgy, Pts 1 and 2, vol. 534-536, 2007, p. 705
[10] Oro, R., et al.: Powder Metallurgy, vol. 55, 2012, p. 294
[11] Oro, R., et al.: Powder Metallurgy, vol. 59, 2016, p. 31
[12] Höganäs AB, Höganäs Iron and Steel Powders for Sintered Components. Höganäs, Sweden, 2002
[13] Metal Powder Industries Federation, Materials Standards for PM Structural Parts, Princeton, New Jersey 08540-6692 U.S.A 2016

Powder Metallurgy Progress, Vol.18 (2018), No.2, p.128-138
http://dx.doi.org/10.1515/pmp-2018-0015

NOVEL HIGH-PERFORMANCE CVD COATINGS FOR MACHINING APPLICATIONS

R. Haubner, E. Rauchenwald, M. Lessiak, R. Pitonak, R. Weissenbacher

Abstract

Investigations of hard and wear resistant materials have a long tradition to increase the performance and profitability of machining applications. The evolution started with WC-Co hardmetal alloys, which were produced by PM technology, followed by CVD coatings on hardmetal tools. The first CVD coatings applied were TiC, TiN and Al_2O_3. The properties of these coatings could be optimized by varying the crystal size, crystal orientation but also combination of the materials in multilayer systems. Nowadays, about 85% of all hardmetal tools are coated.During the last years, driven by PVD coatings showing good performance (e.g. TiAlN), the search for new CVD coatings was intensified. Medium temperature (MT) CVD processes for TiCN allowed the deposition of TiCN crystals with different composition side by side. Due to this microstructure the adhesion between single layers in new multilayer coatings like TiN/MT-TiCN/Al_2O_3/TiN could be increased.

Novel (Ti,Al)N coatings were developed, showing a nanolamellae microstructure consisting of self-assembled (Ti,Al)N with different composition.

For the future there is still plenty to investigate. The already existing coatings and coating systems have to be optimized for the various machining applications. To find new types of CVD coatings, we look for chemical reactions practicable for its use in CVD equipment.

Kewords: CVD, hardmetal, coatings, nanostructures.

INTRODUCTION

Chemical Vapour Deposition (CVD) for hard materials started in the 1930s, when Moers [1] investigated the deposition of TiC. About twenty years later Pollard, Woodward [2] and Münster, Ruppert [3] deposited the first TiC coatings on steel. After further 20 years Krupp Widia launched the first commercial TiC coating on hardmetal tools. Prof. Richard Kieffer started in the 1970s at the "Technische Hochschule Wien" with CVD of TiN [4]. The next important invention was the CVD process for α-Al_2O_3, by Benno Lux´s group at Battelle Geneva, Switzerland. Sandvik Coromant took over these patents in 1971 [5]. The further progress was rapid and many different coatings and combinations of coatings called multilayers were developed [6, 7].

Roland Haubner, Elisabeth Rauchenwald: Technische Universität Wien, Institute of Chemical Technologies and Analytics, Getreidemarkt 9/164-CT, A-1060 Vienna, Austria
Mario Lessiak, Reinhard Pitonak, Ronald Weissenbacher: Boehlerit GmbH & Co. KG, Forschung & Entwicklung, Werk VI Straße 100, A-8605 Kapfenberg, Austria

THE CVD PROCESS

The CVD processes are relatively simple regarding the reactor equipment, gas supply and power supply. Compared to PVD (Physical Vapour Deposition) the throughput of samples in CVD processes is much higher, due to the larger reactor volume [8, 9]. In Fig.1a the production reactor at Boehlerit is shown.

A disadvantage of CVD for hard coatings is the rather high process temperature needed to activate the chemical reactions, and deposit the hard coatings [10]. In Fig.1b the temperature ranges of CVD and PVD processes are summarized. Conventional HT-CVD (high-temperature) works around 1000°C. If precursors with a higher reactivity are used the temperatures can be decreased to about 800°C for MT-CVD (medium temperature), or LT-CVD (low temperature) at around 700°C.

Additionally the chemical reactions cannot be individually influenced in the large reactors. For each coating the chemical reactions have to be designed specifically to guarantee similar coating properties all over the reactor. Once the coating process is optimized, CVD coatings are much cheaper compared to PVD.

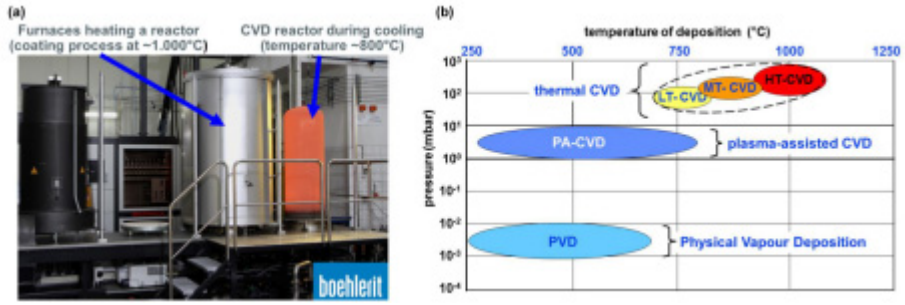

Fig.1. CVD equipment (a); substrate temperature ranges for the deposition processes (b).

HARD COATINGS AND POSSIBILITIES FOR THEIR IMPROVEMENT

For hard coatings on cutting tools several factors have to be considered starting with the tool substrate, the interface to the coating, the properties of the coating itself and the interactions of the coating with the work piece (Fig.2). The properties of the most important materials used for hard coatings are summarized in Tab. 1.

Due to the absence of property changes during the coating process, CVD coated tools are mostly made out of hardmetal alloys (WC-Co). In contrast the microstructure and properties of steel substrates are destroyed at high temperatures.

The interface between substrate and coating is important for the coating adhesion. Differences between thermal expansion coefficients lead to stress at the interface, which can reduce adhesion. Additionally the interface of coatings and its properties are determined during the nucleation phase of the crystal growth, respectively the layer formation. Therefore diffusion and the formation of interlayers have effects too.

The microstructure of coatings is influenced by the deposition parameters, e.g. deposition temperature, concentrations of precursors, gas pressure and gas flow. Additionally the coating performance can be increased by changing the crystal size, the chemical composition and the phase composition of the coatings. Three options to increase wear properties of hard materials can be distinguished.

- Crystalline phases representing solid solutions of two individual phases (solid solution mixed crystals – ss-mixed crystals) [11, 12].
- A decrease in crystallite size increases hardness, because the grain boundaries inhibit the deformation of crystals and crystallographic cracking is reduced.
- Composite mixtures of different phases in one coating. If this mixture is within one layer, the grain size of the crystals is of interest and nano-composites are aspired.

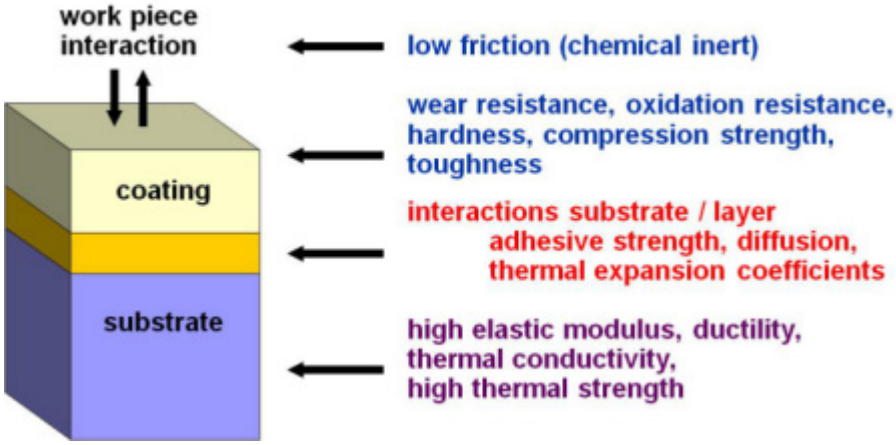

Fig.2. Criteria for the selection of CVD coatings.

Tab.1. Properties and applications of conventional hard coatings.

coating	**TiC**	**TiN**	**TiCN**	**α-Al_2O_3**
	first CVD coating for wear applications			low thermal conductivity
structure	cubic	cubic	cubic	trigonal
hardness HV	2800 - 3200	2200 - 2400	2500 - 2800	2400 - 2600
colour	gray – black	gold – yellow	gray – red – yellow	colourless, transparent
max.ox.res.	600°C	800°C	700°C	1900°C
production	CVD and PVD	CVD and PVD	CVD and PVD	CVD
areas of wear application	combined with other hard coatings decorative coatings	single layers for drilling with cooling intermediate layer to increase adhesion decorative coatings	low flank wear during cutting and milling decorative coatings	cutting and milling of steel best thermal isolation >1000°C

max.ox.res, = maximal oxidation resistance; HV = Vickers hardness
Ti based coatings – TiC, TiN, Ti(C,N)

For carbides and nitrides the chemical reactions are simple and by controlling the precursor concentrations homogeneous deposition is possible even in large industrial reactors. As carrier gases hydrogen or argon can be used.

$$TiCl_4 + CH_4 \rightarrow 2\ TiC + 4\ HCl$$
$$2\ TiCl_4 + N_2 + 4\ H_2 \rightarrow 2\ TiN + 8\ HCl$$

These reactions can also be used for hard coatings containing Zr, Hf and Ta. The differences in the deposition processes are mainly determined by the chemical properties and the vapor pressure of the used precursors [13 - 17].

By adding carbon and nitrogen compounds simultaneously, various TiCN mixtures can easily be deposited (Fig.3). It is also possible to use organic compounds containing both elements (e.g. acetonitrile [18]) as precursors to set the C:N ratio and to allow deposition at medium temperature (MT). In Fig.3 the influence of the deposition conditions on various surface morphologies of coatings is shown. Fig.4 shows the effect of deposition time on the coating surface. It is evident that the surface morphology of coatings influences the interface between different coatings in case of multilayers.

As an additional example in Fig.5 ZrN coatings are shown deposited at 900°C using NH_3 as nitrogen source [19].

$$2\ ZrCl_4 + 2\ NH_3 + H_2 \rightarrow 2\ ZrN + 8\ HCl$$

The various microstructures of the coatings are caused by the different amounts of ammonia added. Different colors are caused by the sample position in the reactor due to slight inhomogeneities in the deposition parameters. Other Zr containing coatings were shown by several researchers [20, 21].

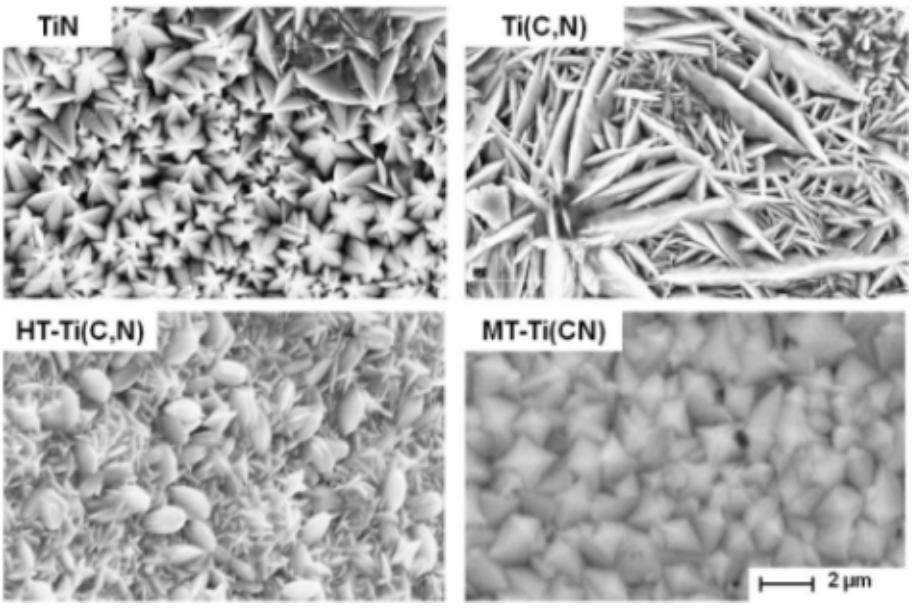

Fig.3. Various surface morphologies of TiN respectively TiCN coatings (Boehlerit GmbH).

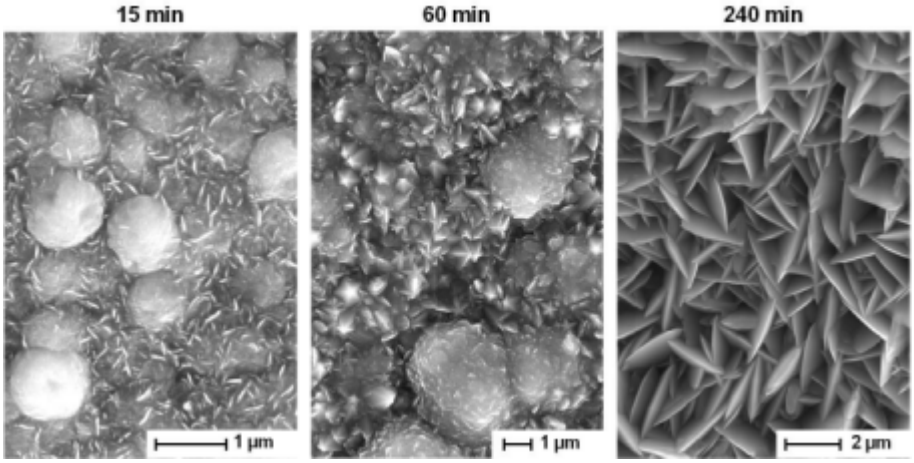

Fig.4. Influence of deposition time on the morphology of HT-TiCN coatings (Boehlerit GmbH).

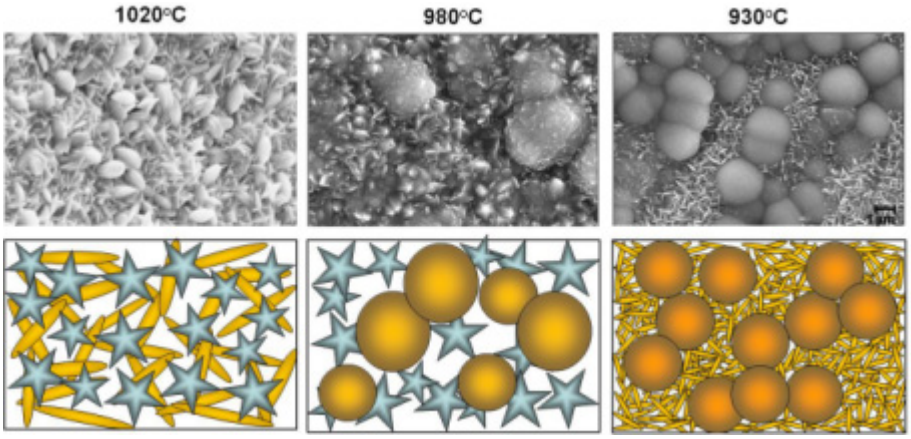

Fig.5. Influence of the deposition temperature on the morphology respectively microstructure of HT-TiCN. Basis of the nanolock coating from Boehlerit.

Simultaneous deposition of two phases by CVD

First investigations for simultaneous deposition of hard materials were executed with Al_2O_3 and TiC [31]. Due to the rather different chemical reactions for Al_2O_3 and TiC by CVD it was not possible to deposit mixed layers of high quality and up-scaling for industrial production was impossible. Later the simultaneous deposition of TiC and TiB_2 was successful on laboratory scale but again these coatings were not realized for industrial applications [21].

The TiCN based Boehlerit coating „NANOLOCK“

A breakthrough for mixed layers was reached by reducing the crystal size of both phases to the range of nanometers. By changing the CVD deposition parameters it was possible to influence nucleation and growth of TiCN crystals with different composition.

This yielded in a specific microstructures and surface morphologies (Fig.5.) [32]. A core-shell structure was formed with higher Nitrogen concentrations in the core and higher Carbon concentrations in the shell respectively [33]. These types of coatings show best results for tube deburring and continuous turning of steel [34]. Due to its good adhesion to subsequent coatings it was named "nanolock".

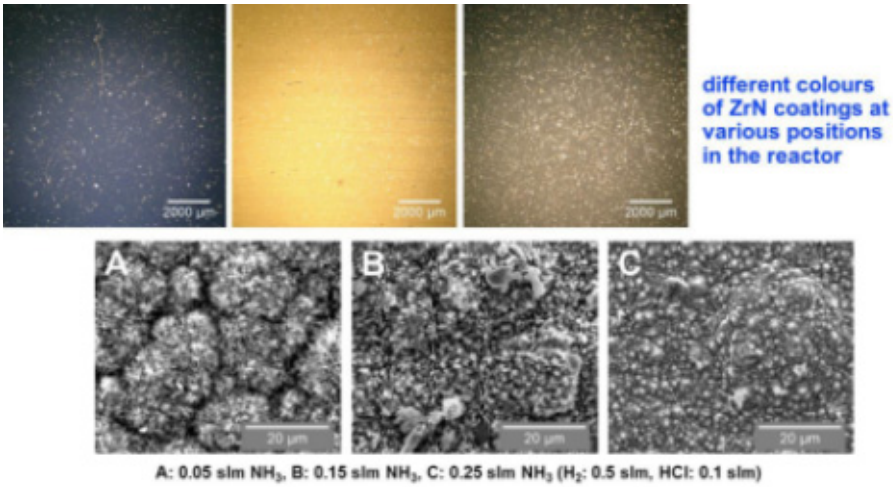

Fig.6. ZrN coatings deposited at 900°C.

Corundum, α-Al_2O_3 coating

The corundum coating is most important for machining steel, due to its low thermal conductivity and high oxidation resistance. The α-Al_2O_3 deposition process has to be performed above 1000°C to achieve the corundum phase. For the coating formation it is not possible to introduce the precursors ($AlCl_3$ and H_2O) directly in the reactor, because of powder formation. To permit the slowly formation of H_2O the reverse watergas shift reaction ($CO_2 + H_2 \rightarrow H_2O + CO$) is used (Fig.3) [22, 23, 24].

In various works nucleation and growth of α-Al_2O_3 on different substrates [25] and the use of different precursors was studied [26]. In addition the conditions and parameters for Al_2O_3 deposition were optimized for industrial processes [27]. During this research it was found that H_2S addition to the process results in more homogeneous coatings. This can be explained by influences on the reaction kinetic of the reverse watergas shift reaction [28]. To modify the microstructure of the α-Al_2O_3 coatings also the effect of impurities was investigated [29, 30].

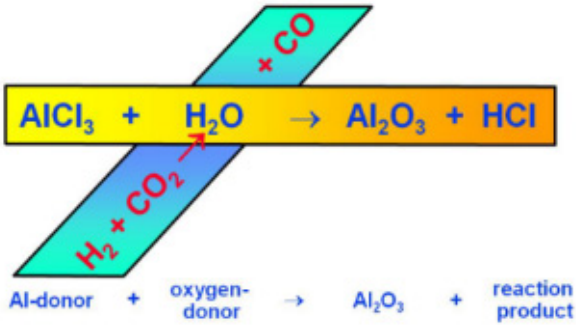

Fig.7. Chemical reactions involved in the deposition of α-Al_2O_3 coatings by CVD.

Coatings containing nano-crystalline lamellae of different (TiAl)N phases

At first coatings containing mixtures of Al and Ti were realized by the invention of (TiAl)N PVD-coatings [35, 36]. These coatings are composed of homogeneous mixed crystals which pass through a spinodal decomposition, into TiN and AlN at increased temperatures [37]. This is responsible for the so called age hardening effect of (TiAl)N and the high performance in milling operations.

To realize the advantages of CVD for industrial mass production, a process for the deposition of (TiAl)N was investigated and realized [38, 39]. This special coating is deposited by MT-CVD at temperatures <850°C and pressures <50 mbar. The overall reaction for the deposition of AlTiN is:

$$3\ TiCl_4 + 3\ AlCl_3 + 7\ NH_3 \rightarrow 3\ AlTiN + 21\ HCl + 2\ N_2$$

Due to higher Al concentrations in these coatings the material is called (AlTi)N. Intense TEM investigations pointed out that not a single phase was deposited but a nano lamellar composite (Fig.8.) [40]. Different phases (w-AlN, c-(TiAl)N or h-(TiAl)N) with a spacing between 6 and 8 nm were measured. The detailed chemistry of the CVD mechanism requires further investigation; however the coating shows high performance in milling of cast iron and steel to which point two milling grades have already been launched on the market.

Multilayer coatings to optimize the wear resistance

Wear resistance and tool life are strongly influenced by the machining conditions and the correlations are complex. New coating sequences are created to increase the performance of tools for selected applications [41, 42].

At first multilayers were deposited to increase the adhesion between substrate and coating. α-Al_2O_3 layers deposited directly on hardmetal tools exhibit a low adhesion, therefore an intermediate TiC layer was deposited [43].

Another reason for the use of multilayers is the reduction of the crystal size within the coatings. During every change in the material new nucleation of crystals is promoted, resulting in a smoother surface or rather smaller roughness [44]. Furthermore the internal stresses caused by different thermal expansion coefficients of substrate and coating materials can be balanced [45].

In praxis it is hard to distinguish which reason is dominant for the good performance of a multilayer coating. In Fig.9 a typical multilayer coating for cutting operations is shown. The nanolock coating described above is located below the α-Al_2O_3 layers. Fig.10 shows the evolution of industrial multilayer coatings with time for cutting operations of steel.

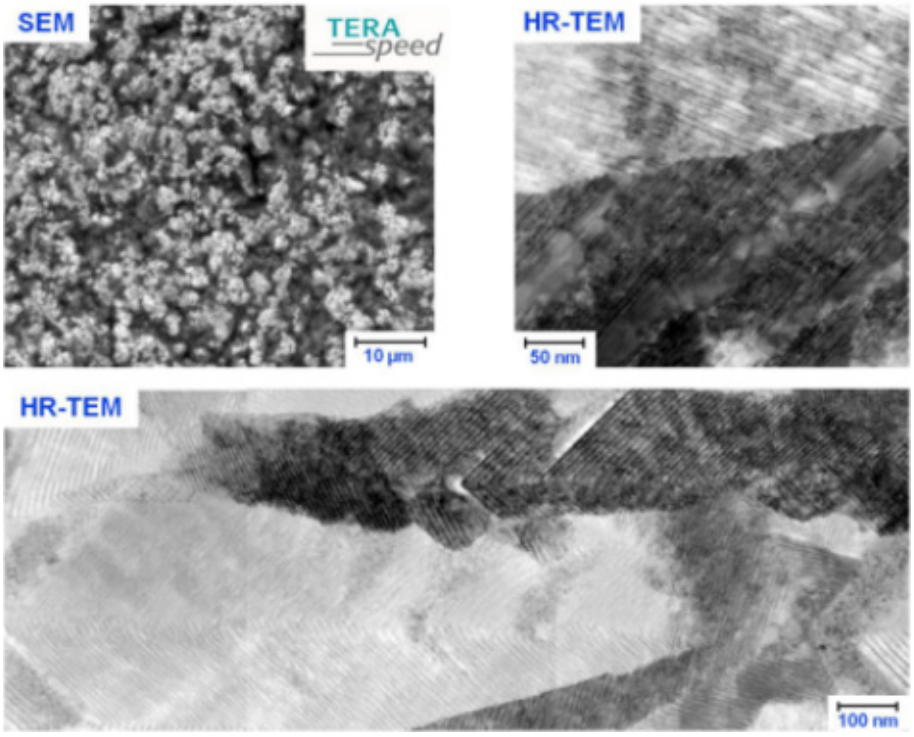

Fig.8. CVD (AlTi)N coating with nano-lamellar microstructure (Boehlerit GmbH).

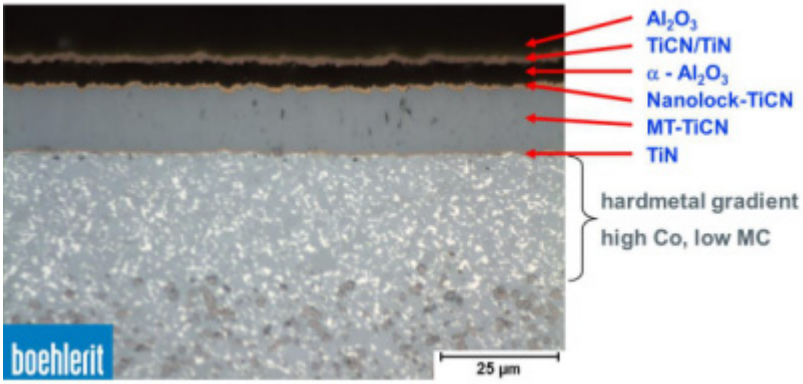

Fig.9. Typical CVD multilayer for cutting applications.

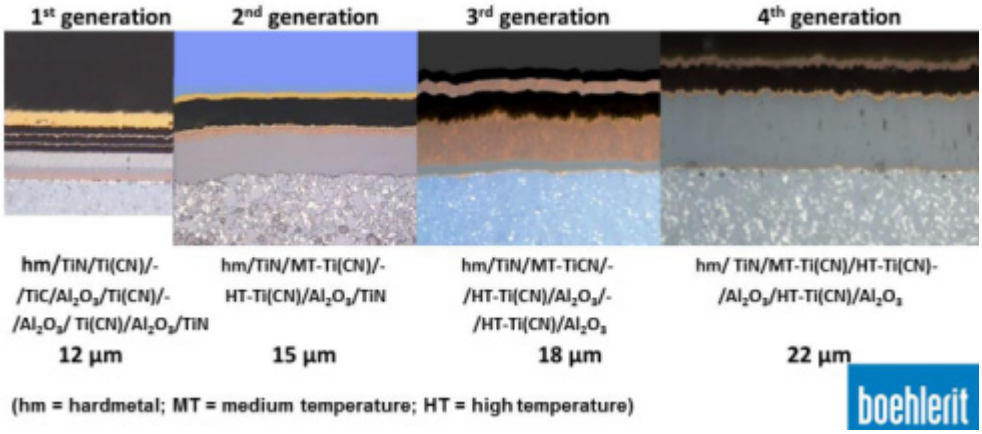

Fig.10. Evolution of CVD multilayer coatings on hardmetal substrates for cutting steel.

CONCLUSION

In spite of the long history of CVD coatings there are still challenges for further research. The deposition of novel ss-mixed crystals, nano-crystalline materials or nano-crystalline mixtures of phases can result in interesting properties of coatings and open the door for new applications. For CVD coatings we have to consider, that for every change in the chemical reactions the deposition parameters have to be newly optimized. Therefore a good cooperation between research institutes and industry is helpfull to investigate novel and unique coatings respectively products.

Acknowledgement

At first we like to thank Prof. Benno Lux [46] who introduced CVD at the TU Wien. Our thanks also go to the various Austrian Science Foundations for financing projects over many years. Last but not least we would like to thank all the students and researchers working at universities and in companies on various projects.

REFERENCES

[1] Moers, K.: Z. anorg. und allgem. Chemie, vol. 198, 1931, p. 243
[2] Pollard, FH., Woodward, P.: Trans. Faraday Soc., vol. 46, 1950, p. 190
[3] Münster, A., Ruppert, WZ.: Elektrochem., vol. 57, 1953, p. 564
[4] Haubner, R.: Int. J. Refract. Met. Hard Mater., vol. 41, 2013, p. 22
[5] Lux, B., Funk, R., Schachner, H., Triquet, C.: CH Expose D'Invention 540990; 7.7.1971
[6] Kornmann, M., Schachner, H., Funk, R., Lux, B.: J. Cryst. Growth, vol. 28, 1975, p. 259
[7] Funk, R., Schachner, H., Triquet, C., Kornmann, M., Lux, B.: J. Electrochem. Soc., vol. 123, 1976, p. 285
[8] Lux, B., Haubner, R., Altena, H., Colombier, C. In: Hartstoffschichten zur Verschleißminderung. Eds. H. Fischmeister, H. Jehn. DGM Informationsgesellschaft, 1987, p. 71
[9] Choy, KL.: Progress in materials science, vol. 48, 2003, p. 57
[10] Haubner, R., Lux, B. In: Pulvermetallurgie in Wissenschaft und Praxis. Band 13. Ed. R. Ruthardt. Werkstoff-Informationsgesellschaft, 1997, p. 89

[11] Hollek, H. In: Metallkundlich-Technische Reihe, 6. Ed. G. Petzow. Berlin, Stuttgart : Gebrüder Borntraeger, 1984
[12] Hollek, H. In: Hartstoffschichten zur Verschleißminderung. Eds. H. Fischmeister, H. Jehn. DGM Informationsgesellschaft, 1987, p. 25
[13] Bull, SJ., Bhat, DG., Staia, MH.: Surf. Coat. Technol., vol. 163-164, 2003, p. 499
[14] Bull, SJ., Bhat, DG., Staia, MH.: Surf. Coat. Technol., vol. 163-164, 2003, p. 507
[15] Oakes, J.: Thin Solid Films, vol. 107, 1983, p. 159
[16] Wohlrab, C., Haubner, R., Schintlmeister, W., Lux, B.: Int. J. Refract. Met. Hard Mater., vol. 9, 1990, p. 192
[17] Lessiak, M., Haubner, R., Pitonak, R., Köpf, A., Weissenbacher, R.: Physica Status Solidi C, vol. 12, 2015, p. 1043
[18] Bonetti-Lang, M., Bonetti, R., Hintermann, HE. In: Proc 8th Int Conf on CVD, 1981, p. 606
[19] Rauchenwald, E., Lessiak, M., Weissenbacher, R., Haubner, R.: (to be published).
[20] Osada, A., Danzinger, M., Haubner, R., Lux, B.: Journal de Physique IV, Coll.C2, vol. 1, 1991, p. 557
[21] Iiyoshi, H.: Doctoral Thesis. Vienna : TU, 1990
[22] Altena, H., Lux, B.: Int. J. Refract. Met. Hard Mater., vol. 6, 1987, p. 53
[23] Peng, J., Danzinger, M., Lux, B.: Int. J. Refract. Met. Hard Mater., vol. 10, 1991, p. 203
[24] Ruppi, S.: Int. J. Refract. Met. Hard Mater., vol. 23, 2005, p. 306
[25] Altena, H., Colombier, C., Lux, B. In: Proc of the 4th Europ Conf on CVD. Eds. J. Bloem , G. Verspui, L. Wolff. Eindhoven, 1983, p. 435
[26] Colombier, C., Lindström, J., Lux, B.: Int. J. Refract. Met. Hard Mater., vol. 5, 1986, p. 222
[27] Altena, H., Stjernberg, K., Lux, B. In: Proc Euro-CVD-Five. Uppsala, Sweden, 1985, p. 381
[28] Blomqvist, A., Århammar, C., Pedersen, H., Silvearv, F., Norgren, S., Ahuja, R.: Surf. Coat. Technol., vol. 206, 2011, p. 1771
[29] Danzinger, M., Peng, J., Haubner, R., Lux B.: Journal de Physique IV, Coll.C2, vol. 1, 1991, p. 571
[30] Danzinger, M., Haubner, R., Lux, B.: Int. J. Refract. Met. Hard Mater., vol. 14, 1996, p. 69
[31] Colombier, C., Lux, B.: Journal of Materials Science, vol. 24, 1989, p. 462
[32] Garcia, J., Pitonak, R., Agudo, L., Kostka, A.: Materials Letters, vol. 68, 2012, p. 71
[33] Garcia, J., Pitonak, R., Weissenbacher, R., Köpf, A.: Surf. Coat. Technol., vol. 205, 2010, p. 2322
[34] Garcia, J., Pitonak, R.: Int. J. Refract. Met. Hard Mater., vol. 36, 2013, p. 52
[35] Knotek, O., Bohmer, M., Leyendecker, T.: J. Vac. Technol. A, vol. 4, 1986, p. 2695
[36] Jehn, HA., Hofmann, S., Ruckborn, VE., Munz, WD.: J. Vac. Technol. A, vol. 4, 1986, p. 2701
[37] Mayrhofer, PH., Music, D., Schneider, JM.: Appl. Phys. Lett., vol. 88, 2006, p. 1
[38] Endler, I., Hermann, M., Naupert, M., Pitonak, R., Schneider, M., Van den Berg, H., Westphal, H., Ruppi, S. In: Proceedings EuroPM 2006. Gent, Belgium p. 219
[39] Pitonak, R., Köpf, A., Weissenbacher, R., Keckes, J., Stefenelli, M., Todt, J., Endler, I., Höhn, M. In: Proc of the 18th Plansee Seminar 2013. Reutte, HM37/1-12
[40] Keckes, J., Daniel, R., Mitterer, C., Matko, I., Sartory, B., Köpf, A., Weissenbacher, R., Pitonak, R.: Thin Solid Films, vol. 545, 2013, p. 29
[41] Undercoffer, KE., Downey, BK., Battaglia, FB., Bryant, WA. In: Proc 7th Euro Conf.

on CVD 1989, C5, p. 783
[42] Halvarsson, M., Larsson, A., Rupi, S.: Micron, vol. 32, 2001, p. 807
[43] Lindström, J., Johnsson, BF., Ohlson, FJ.: German Patent P2443160.5-14 (10.9.1974)
[44] Garcia, J., Pitonak, R., Weißenbacher, R., Köpf, A., Soldera, F., Suarez, S., Miguel, F., Pinto, H., Kostka, A., Mücklich, F.: Advanced Engineering Materials, vol. 12-9, 2010, p. 929
[45] Dobrzański, LA., Skrzypek, S., Pakuła, D., Mikuła, J., Křiž, A.: Journal of Achievements in Materials and Manufacturing Engineering, vol. 35/2, 2009, p. 162
[46] Ortner, HM., Haubner, R.: Int. J. Refract. Met. Hard Mater., vol. 41, 2013, p. 1